Earth and Planetary Science Letters 531 (2020) 115989

Contents lists available at ScienceDirect

Earth and Planetary Science Letters

www.elsevier.com/locate/epsl

Repeated magmatic buildup and deep "hot zones" in continental evolution: The Cadomian crust of Iran

Hadi Shafaii Moghadam [a,b,c,*,**], Q.L. Li [a,*], W.L. Griffin [c], R.J. Stern [d], O. Ishizuka [e,f], H. Henry [c], F. Lucci [g], S.Y. O'Reilly [c], G. Ghorbani [b]

[a] State Key Laboratory of Lithospheric Evolution, Institute of Geology and Geophysics, Chinese Academy of Sciences, Beijing 100029, China
[b] School of Earth Sciences, Damghan University, Damghan 36716-41167, Iran
[c] Arc Centre of Excellence for Core to Crust Fluid Systems and GEMOC ARC National Key Centre, Dept. of Earth and Planetary Sciences, Macquarie University, NSW 2109, Australia
[d] Geosciences Dept. University of Texas at Dallas, Richardson, TX 75083-0688, USA
[e] Japan Agency for Marine-Earth Science and Technology, 2-15 Natsushimacho, Yokosuka, Kanagawa, 237-0061, Japan
[f] Geological Survey of Japan/AIST, Tsukuba, Ibaraki, 305-8567, Japan
[g] Dipartimento di Scienze, Sezione Scienze Geologiche, Università "Roma Tre", 1-00146 Rome, Italy

ARTICLE INFO

Article history:
Received 11 July 2019
Received in revised form 29 October 2019
Accepted 26 November 2019
Available online 5 December 2019
Editor: A. Yin

Keywords:
continental crust
magmatic flare-up
hot zone
Cadomian
Iran

ABSTRACT

The generation and differentiation of continental crust by arc magmatism is strongly influenced by episodes of high magmatic flux ("flare-ups"). Magmatic flare-ups encourage the development of deep crustal hot zones where magmatic differentiation and density stratification combine to form the upper felsic and lower mafic continental crust. Such processes, which are responsible for the construction of continental arc crust, are prolonged events, which build a ~30-40 km arc crust over tens of million years (~100 Myr). New zircon U-Pb data reveal that the construction of Cadomian crust from NE Iran occurred over ~15 ± 0.3 Myr. However, compiled zircon U-Pb ages reveal a prolonged magmatic flare-up of ~45 Myr; ~570 to 525 Ma. Basement outcrops in NE Iran expose lower- and upper crust that show how magmatic-geochemical differentiation occurred deep beneath a Cadomian continental arc in a crustal hot zone. Isotopic data for igneous rocks produced during this 45 Myr episode reveal interactions between mantle-derived melts and old continental crust. Synthesis of new and published data indicates that this type of interaction is common during periods of high magmatic fluxes. Our results indicate that differentiation of mafic melts in the lower crust during prolonged magmatic flare-ups plays a key role in building a stratified continental crust.

1. Introduction

Subduction-related magmatism along active continental margins is regarded as one of the main mechanisms for the generation of magmatic pulses within the continental crust. However, the controlling factors and time-scales producing compositional diversification within most arcs remain controversial. Arc magmatism in most subduction zones is a prolonged process, which builds a ~30-40 km arc crust over tens of millions of years (~100 Myr for continental arcs *vs* ~40 Myr for oceanic ones, Ducea et al., 2015b), although recent zircon U-Pb observations on the Sierra Valle Fertile crustal section (Famatinian arc, Argentina), show that the entire arc crust (~30 km thickness) can be built by magmatic processes within ~4 Ma (Ducea et al., 2017). These short-lived magmatic processes are responsible for the construction of continental crust in some modern arcs (Jicha and Jagoutz, 2015), but their role in the building of crust in ancient arcs, such as the Neoproterozoic-Early Cambrian arcs from northern Gondwana, is enigmatic. The other ambiguities we want to understand are the mechanisms that control the lower-middle crustal diversification in ancient arcs. Both short-lived and prolonged magmatism in most arcs is accompanied by high-magmatic fluxes ("flare-ups") and the removal of the deep lithosphere by delamination (Ducea et al., 2015a, 2015b).

Seismic-velocity measurements suggest that the lower- and middle crust of continental arcs is composed chiefly of gabbroic and intermediate tonalitic rocks and their metamorphic equivalents (Kitamura et al., 2003). The composition and flux of mantle-derived magmas and the processes operating on these to produce

* Corresponding authors.
** Corresponding author at: FB4–Dynamics of the Ocean Floor, GEOMAR, Helmholtz-Zentrum für Ozeanforschung Kiel, Wischhofstr. 1-3, 24148 Kiel, Germany.
E-mail addresses: hshafaei@geomar.de (H. Shafaii Moghadam), liqiuli@mail.iggcas.ac.cn (Q.L. Li).

https://doi.org/10.1016/j.epsl.2019.115989

lower continental crust through continental arc magmatism have been investigated experimentally (Christensen and Mooney, 1995) and by petrological and geochemical modeling (Jagoutz, 2014). Magmatic differentiation occurs at intermediate crustal levels (~20-30 km deep), mostly associated with large intrusions of intermediate to felsic composition, and in lower-crustal "deep crustal hot zones" (Annen et al., 2006) and/or mafic zones (Walker et al., 2015), where differentiating mantle-derived magmas interact with pre-existing crust, in MASH (combined Mixing, Assimilation, Storage and Homogenization) zones. Lower-crustal MASH processes can also be linked to the foundering of ultramafic-mafic cumulates and residues back into the mantle.

Studying lower crustal arc sections is difficult, but is possible in some places, for example Kohistan and Talkeetna. The Kohistan area (NE Pakistan) exposes juvenile continental crust formed in an Early Cretaceous oceanic arc (Jagoutz and Schmidt, 2012). Further evidence for magmatic stratification beneath arc roots comes from observations of the Jurassic Talkeetna continental arc (south-central Alaska) (Behn and Kelemen, 2006), the late Paleozoic Cabo Ortegal complex (Spain) (Tilhac et al., 2016), and the Ordovician Famatina Complex of Argentina (Ducea et al., 2017; Walker et al., 2015). The aim of this study is to utilize these and other insights to evaluate the role of different magmatic fluxes in forming a differentiated crust and to better understand how the continental crust of Iran formed. This crust mostly formed in Late Ediacaran and Early Cambrian time during an episode known in Europe as the Cadomian orogeny. We focus on exposures around Torud in NE Iran (Fig. 1), where lower crust and complementary upper crust are exposed, providing a quasi-continuous exposure of a Cadomian continental magmatic arc. Our results indicate that magmatic differentiation occurred predominantly in the deep crust beneath this arc, during a flare-up event. Our results strongly support the idea that deep crustal "hot zones" existed beneath such arcs, where mafic melts differentiated, and further suggest that lower-crustal foundering associated with the hot zone was incomplete. We also show that the Cadomian arc crust of Iran was entirely formed by magmatic processes within ~15 Myr, which is significantly longer than in modern arcs.

2. Geological background

The Cadomian orogen of Europe, SW Asia (Iran and Anatolia) and E. North America was a Late Ediacaran to Early Cambrian peripheral accretionary margin and magmatic arc generated above a south-dipping subduction zone along northern Gondwana (Linnemann et al., 2010). Cadomian arc magmatism in Iran and Anatolia occurred in a transtensional setting above this subduction zone to build the ribbon continent "Cimmeria" which rifted off Gondwana and accreted to Eurasia in late Paleozoic time (Moghadam et al., 2015). Cadomian arc magmatism generated the continental nuclei of Iran, with a magmatic "flare-up" in latest Ediacaran time (Moghadam et al., 2017d).

Significant exposures of Cadomian magmatic rocks in Iran are known from the west (Golpayegan), northwest (Khoy-Salmas, Zanjan-Takab), northeast (Torud, Taknar) and central regions (Saghand) (Fig. 1A). The Cadomian basement rocks of Iran were mostly exhumed as a result of Cenozoic extension and core-complex formation (Verdel et al., 2007). Cadomian magmatic rocks in Iran and Turkey mostly form felsic plutons (granite to tonalite) along with minor dacitic to rhyolitic extrusive rocks. Intermediate to mafic intrusive rocks are less abundant and basaltic lavas are rare.

Cadomian crust is exposed over about 40,000 km^2 in NE Iran, from NE of Torud to south of Taknar (Fig. 1B). It is overlain by Jurassic and Cretaceous metasedimentary rocks. Ar-Ar and K-Ar ages on muscovite and biotite from NE Iran orthogneisses yield ages of *ca* 160 and 171 Ma, respectively (Rahmati-Ilkhchi et al., 2010), which are interpreted as the ages of metamorphism and exhumation. Recent Ar-Ar data show that the exhumation has occurred during Late Cretaceous time, due to the extensional phases which were affecting the Iranian plateau during that time (Malekpour-Alamdari et al., 2017). Cadomian exposures in NE Iran include a section of middle to upper crust, comprising gabbroic-dioritic intrusions (U-Pb zircon age ~556 Ma) grading into a thick sequence (~20 km) of granitoid intrusions (U-Pb zircon ages ~532-552 Ma) grading upward into felsic volcanic rocks (U-Pb zircon age ~550 Ma) and psammitic to volcanogenic metasediments (with detrital U-Pb zircon ages of ~549-552 Ma) (Moghadam et al., 2015). Felsic and mafic (amphibolite) dikes and sills yield zircon U-Pb ages of *ca* 532-554 Ma (Hosseini et al., 2015). Felsic intrusions comprise I-type granites, granodiorites and tonalites; these are isotopically variable, with initial εNd of −6 to +7, zircon εHf ranging from −9.6 to +10.7 and δ^{18}O of zircon between ~+5 to >+9‰. These isotopic data suggest the involvement of both juvenile melts and older continental crust (Moghadam et al., 2015).

The recently discovered arc section in the Cadomian segment of NE Iran (Torud) integrated with the neighboring crustal exposures, is one of the best quasi-continuous vertical, but tilted deep exposures of a subduction-related Cadomian continental arc crust in Iran. The upper-crustal rocks in this area are dominated by metasediments, including paragneissic rocks and metapelites, grading downward into middle crust dominated by felsic to intermediate intrusions, interlayered with metasedimentary host-rocks. Mafic rocks are also present in the middle crust but are rare. The upper-middle crustal intrusive rocks are mildly to highly deformed and metamorphosed to various types of gneissic rocks, dependent of their composition (e.g., granitic gneisses to dioritic gneisses). Felsic dikes (variably metamorphosed) are abundant in the middle-crustal intrusions.

The middle-upper crustal section changes downward into middle-lower crustal outcrops including amphibole-bearing mafic rocks – now appearing as mylonitic gabbros, meta-gabbroids and amphibolites with a cumulate-like texture; hereafter referred to as cumulate rocks – with a total thickness of ~4 km. Some of these mafic rocks are highly deformed mylonites, whereas some just show slight traces of metamorphism. In this study, we focus on zircon U-Pb ages of magmatic rocks from this Cadomian section and particularly on the cumulate rocks as a likely "deep crustal MASH zone" that was responsible for generating Cadomian middle-upper crust felsic rocks associated with an ~10 Ma long Cadomian arc-crust generation in NE Iran.

3. Analytical methods

Twelve new LA-ICPMS and SIMS zircon ages and Lu-Hf isotope data are reported on middle to lower crustal intrusions, both cumulates and their metamorphic equivalents (metagabbros, mylonitic gabbros and amphibolites) as well as granitic to tonalitic gneisses. We analyzed five samples (those dated by LA-ICPMS) for zircon trace elements and used these data to carry out Ti-in-zircon thermometry. Whole-rock major- and trace elements and Sr-Nd-Pb isotopes, and the compositions of minerals in magmatic rocks are also presented. We used also Electron Back-Scatter Diffraction analysis to investigate the microstructures of the studied rocks. Analytical procedures are described in Appendix A.

4. Results

4.1. Sample descriptions

Field work and sample collection were done on felsic to intermediate metamorphosed intrusions and dikes from the upper-middle crust and on lower crustal cumulate rocks from the area NE of Torud (NE Iran, Fig. 1). The new data presented here are

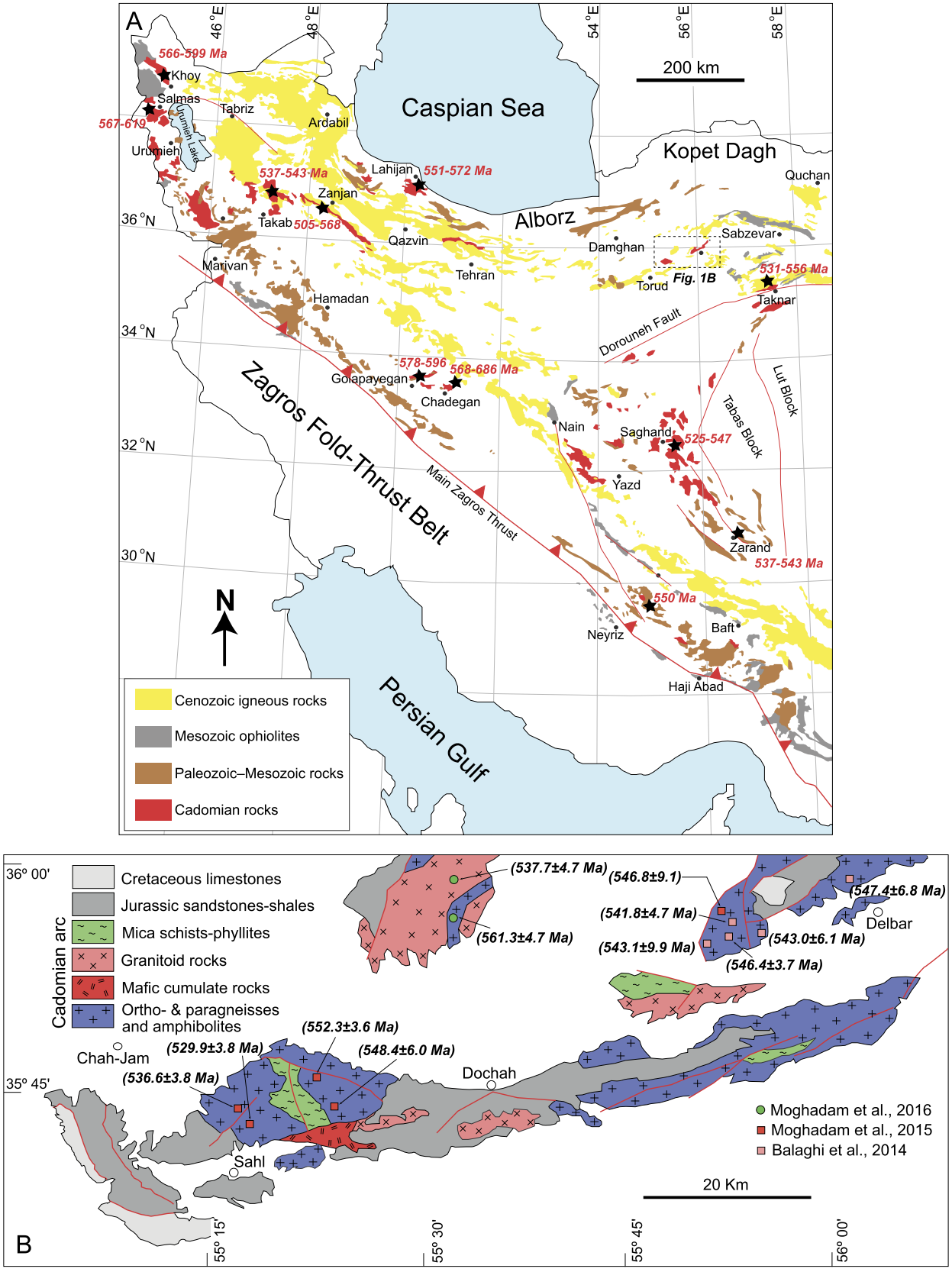

Fig. 1. A - Simplified geological map of Iran showing the distribution of Cenozoic igneous rocks, Mesozoic ophiolites, Paleozoic-Mesozoic igneous rocks and Cadomian basement rocks; the location of the study area is also shown. Cadomian basement makes up most of the crust of Iran. Modified from Moghadam et al. (2017a) with John Wiley and Sons Inc. permission. B - Simplified geological map of NE Iran (Modified after 1/250,000 geological maps of Kharturan and Torud, Geological Survey of Iran) (For interpretation of the colors in the figure(s), the reader is referred to the web version of this article.)

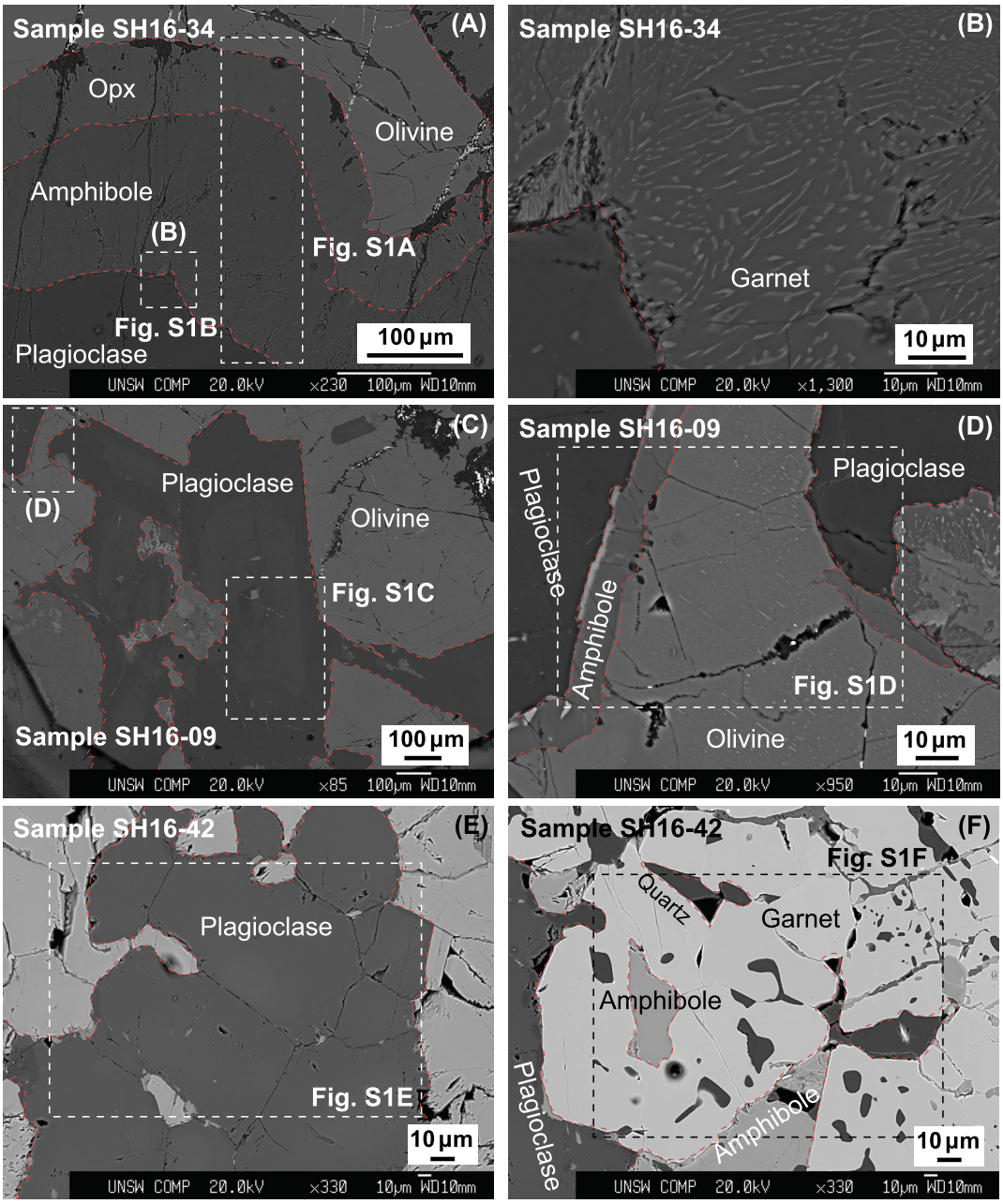

Fig. 2. Back-scattered images showing the symplectite overgrowths between olivine and plagioclase (in sample SH16-34), which composed of orthopyroxene and amphibole (A) with fine-grained vermicular growth of garnet (B). Zoned plagioclase from metagabbros (sample SH16-9) (C) with amphibole corona between olivine and plagioclase (D). Undeformed plagioclases from mylonitic gabbros (E) and garnet porphyroclasts (F) from gneissic granites. Garnets contain quartz and amphibole inclusions. Thin red dashed lines outline the boundaries between different mineral phases.

integrated with other data from Cadomian terranes of NE Iran (Moghadam et al., 2015).

Cadomian cumulate rocks from NE Iran include gabbronorites (olivine + clinopyroxene; Cpx + orthopyroxene; Opx + plagioclase ± spinel), metagabbros (Cpx + amphibole + plagioclase ± olivine ± Opx ± garnet ± quartz ± phlogopite), amphibolites (amphibole + plagioclase ± Cpx ± quartz ± K-feldspar) and metapyroxenites (olivine + altered Cpx + titanomagnetite). Granitic (now granitic gneiss) dikes crosscut these rocks and include quartz + K-feldspar + plagioclase ± garnet ± biotite. Middle-crustal metamorphosed intrusions and their crosscutting dikes comprise granitic to tonalitic gneisses. These rocks contain K-feldspar (orthoclase and microcline) + quartz + plagioclase + biotite ± garnet ± amphibole ± muscovite ± allanite. The detailed petrographic composition of the sampled rocks is presented in Table S1.

Symplectites are present between olivine and plagioclase in metagabbros and comprise thin bands of Opx and thick bands of amphibole (Figs. 2A-S1A). Vermicular garnet is present within the amphibole coronas (Figs. 2B-S1B). Plagioclase in gabbronorites is slightly zoned (Figs. 2C-S1C) and shows a thin amphibole corona at the contact with olivine (Figs. 2D-S1D). Plagioclase from mylonitic gabbros shows slight patchy zonation (Figs. 2E-S1E). Garnets in granitic gneisses are not zoned and include grains of quartz and amphibole (Figs. 2F-S1F).

Granitic gneisses and gabbros reveal varying degrees of deformation. A granitic gneiss (SH16-28) displays deformed quartz (i.e. abundant subgrains and undulose extinction) coexisting with relatively unstrained feldspars (Fig. 3) suggesting this sample underwent plastic deformation. A mylonitic gabbro (sample SH16-42) shows relics of strained clinopyroxenes (~1 mm in grain

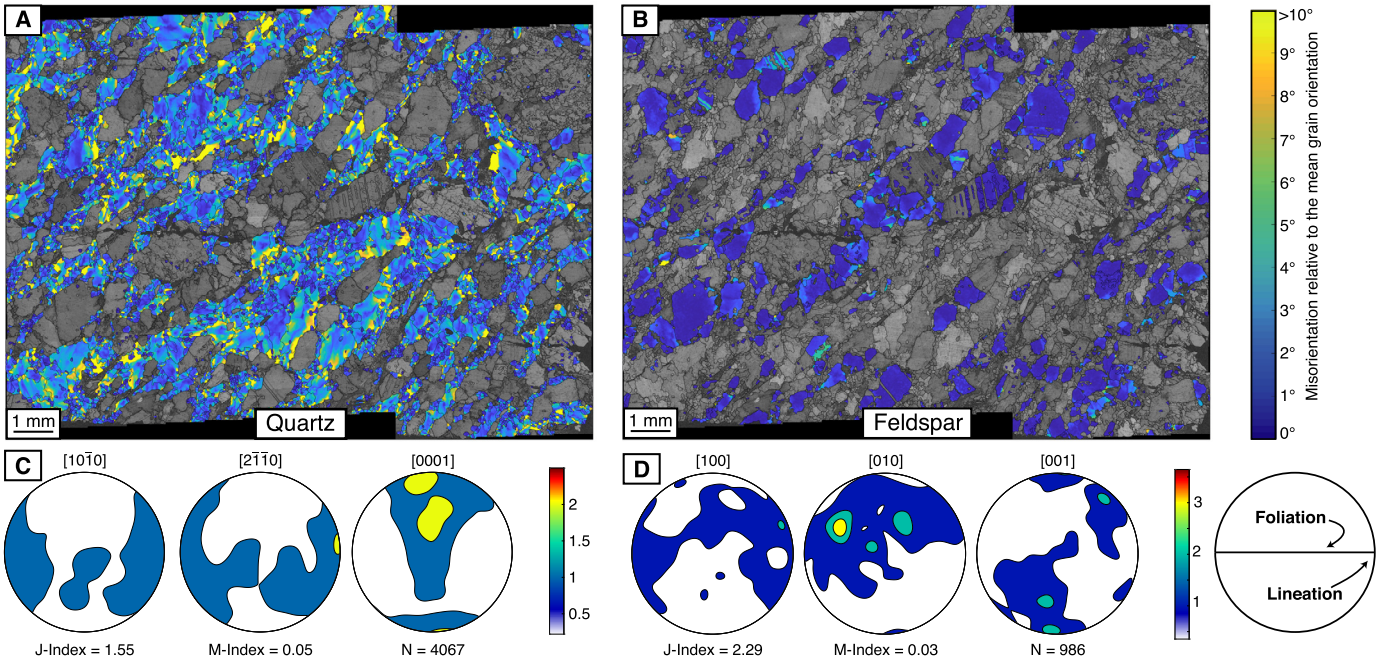

Fig. 3. (A) Map of misorientation to the mean grain orientation for quartz grains from Cadomian granitic gneiss (sample SH16-28). Quartz shows complex grain boundaries, grain boundaries migration and dynamic recrystallization by subgrain rotation. (B) Map of misorientation to the mean grain orientation for feldspar. Feldspars do not show extensive internal misorientation compared to that of the surrounding quartz.

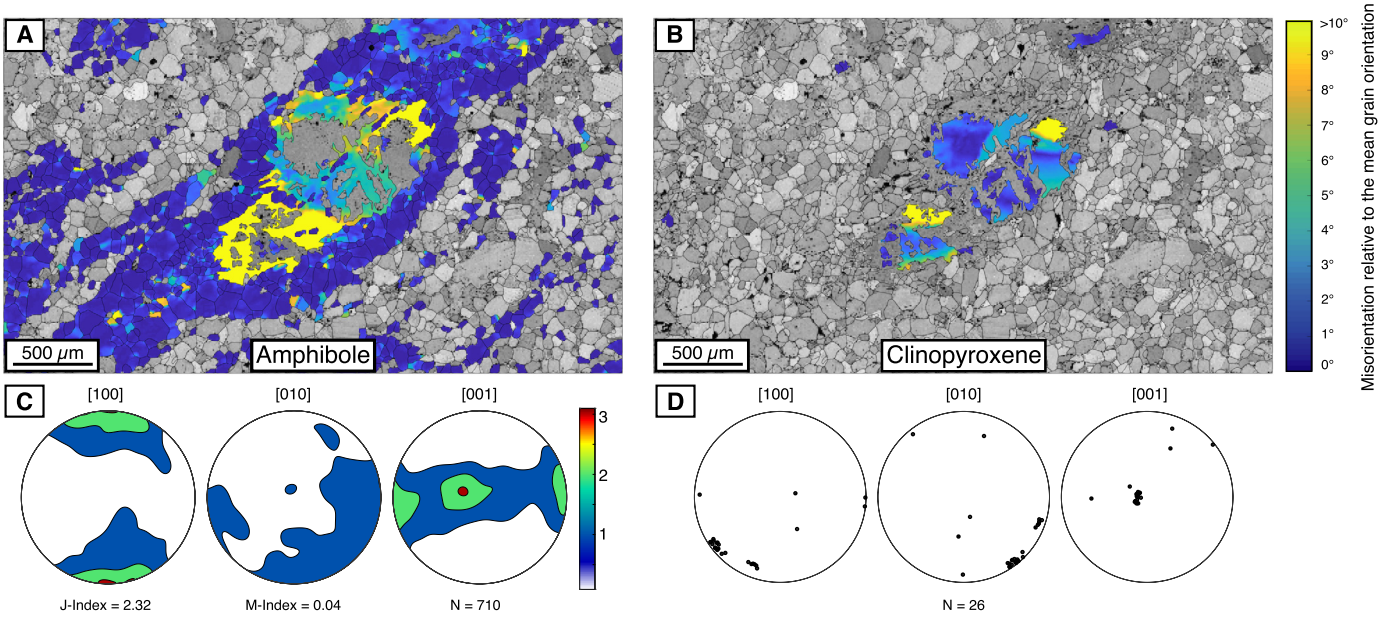

Fig. 4. Map of misorientation to the mean grain orientation for amphiboles (A) and clinopyroxene (B) from mylonitic gabbros (sample SH16-42). Note the important lattice misorientation for the coarse-grained amphibole contrasting with the misorientation-free and texturally equilibrated smaller-grained fraction amphibole. Pole figures for amphibole (C) and clinopyroxene (D) for the same sample. The amphibole [001] axes form two clusters with one of them having a similar direction as that of [001] of clinopyroxene. Clinopyroxene [010] also fall within a similar direction as that of [010] of amphibole. A second cluster of [001] of amphibole is found at a high angle from that of clinopyroxene [001].

size, Fig. 4) surrounded by coarse-grained (~1-2 mm in grain size) amphiboles rich in lattice misorientations. Fine-grained (~50-150 μm in grain size) and unstrained (i.e. 120° triple junctions and misorientation-free) amphiboles surround the larger amphiboles (Fig. 4). Crystallographic preferred orientations of amphibole and clinopyroxene in the mylonitic gabbro are presented in Fig. 4. It displays a crystallographic preferred orientation for the amphibole (J- and M-indices of 2.32 and 0.04). A cluster of amphibole [001] and [010] axes have directions similar to those of Cpx [001] and [010] axes, respectively.

4.2. Mineral compositions

Clinopyroxene from cumulate gabbros is augite (Fig. S2A) with Mg# ~0.8. Orthopyroxene has high Al_2O_3 contents (1.3 to ~2 wt%; Table S2). Olivine has forsterite contents of 69-77%. Cumulate plagioclase has labradorite to bytownite composition, whereas metagabbros and mylonitic gabbros have more sodic plagioclase, in the range of oligoclase-andesine (Fig. S2B). Granodioritic gneisses contain plagioclase with andesine composition. Most amphibole cumulates (and their metamorphic equivalents) are character-

ized by high-Al (Al_2O_3 = 10-15 wt%) pargasitic and magnesio-hornblende compositions, but edenitic and tschermakitic compositions are also common (Fig. S2C). Garnet from mylonitic gabbros has high contents of almandine (55.7%) and grossular (38%) but low pyrope (2.1%) and spessartine (4.1%) endmembers, whereas granitic gneisses have garnets with slightly higher almandine (~56-58%). Garnet in granodioritic gneisses has almandine end-member in the range of 49.3 to 67.7%. Mica in granitic gneisses is biotite (Mg# ~0.2-0.3), whereas mylonitic gabbros carry phlogopite (Mg# ~0.8). Spinels are ferritchromite with high FeO (37-66 wt%) and Cr# 0.2-0.4 (Table S2).

4.3. Zircon U-Pb dating and Hf isotope

Figs. 5 and S3 show the LA-ICPMS and SIMS U-Pb zircon ages obtained in this study for two Cadomian metagabbros, one metagabbronorite, one mylonitic gabbro, one granitic (-gneiss) dike within tonalitic gneisses, one hornblende-bearing metagabbro, one tonalitic gneiss, four granitic to granodioritic gneisses and one granitic (-gneiss) dike within granodioritic gneisses. Details of the U-Pb geochronology are provided below.

4.3.1. Sample SH16-28

This sample is a garnet-bearing granitic gneiss, injected within the Cadomian coarse-grained tonalitic gneisses. The sample contains porphyroblasts of quartz, K-feldspar, plagioclase, biotite and garnet. CL images of zircons revealed neither inherited cores nor metamorphic rims. Zircons are ~150-100 µm long. Most zircons have oscillatory zoning. Zircons separated from this sample contain 115-1713 ppm U, 276-1394 ppm Th and Th/U = 0.2-0.8. We analyzed 38 zircon grains from this sample (Table S3A). Twenty-seven analyses are concordant (Fig. 5) and yield a mean $^{206}Pb/^{238}U$ age of 537.7 ± 2.6 Ma (MSWD = 1.3). This is taken as the crystallization age of this granitic dike. Some zircons have $^{206}Pb/^{238}U$ ages of 541 to 566 Ma (and one grain with 669 Ma) and are considered as antecrystic and xenocrystic zircons.

Sample SH16-28 displays a noteable range of εHf, between −3.4 and −24.7 (Table S5). Corresponding crustal model ages (T_{DM}^C) for zircons from sample SH16-28 vary from 1.7 to 3 Ga.

4.3.2. Samples SH16-14 and SH16-43

These samples are metagabbros with relict plagioclase, amphibole and clinopyroxene. Zircons separated from these samples are large (>100 µm in sample SH16-43) or short prismatic (~70-100 µm in sample SH16-14) and most show oscillatory zoning. Zircons contain 186-4395 ppm U, 159-11666 ppm Th contents and Th/U from 0.3-4.7 (Table S3A). Some zircons have high Th and U content. Out of thirty-five zircon grains analyzed from each samples twenty-two grains yield a mean $^{206}Pb/^{238}U$ age of 542.1 ± 2.5 Ma (MSWD = 1.5; Fig. S3) for sample SH16-14 and twenty-one zircons from SH16-43 give a mean $^{206}Pb/^{238}U$ age of 534.3 ± 2.1 Ma (MSWD = 2). These ages (~542-534) are taken as the crystallization ages of the gabbros. Some other zircons show $^{206}Pb/^{238}U$ ages of >547 Ma and up to 624 Ma, which are considered as both antecrystic and inherited zircons. Sample SH16-43 includes a few zircons with high U and Th contents, and these zircons show younger ages of 505 and 509 Ma. We have deleted these younger ages from age interpretation of this sample, as they probably are related to destruction of the zircon structure and Pb loss due to the high U and Th abundances.

Sample SH16-43 displays a notable range of εHf, between +2.7 and +9.2 (Table S5). Corresponding crustal model ages (T_{DM}^C) for zircons from sample SH16-43 vary from 0.9 to 1.3 Ga. Sample SH16-14 has zircon εHf ranging from +6.9 to −0.2, lower than the εHf values of zircons in sample SH16-43. Corresponding T_{DM}^C for zircons from sample SH16-14 vary from 1.1 to 1.5 Ga.

4.3.3. Sample SH16-17

This sample is a foliated hornblende-bearing metagabbro. The sample contains coarse-grained relict amphibole, plagioclase, quartz with clinopyroxene. CL images of zircons revealed neither inherited cores nor metamorphic rims. Zircons are short prismatic, and ~50-70 µm long. Most zircons are homogeneous and lack oscillatory zoning, except in the grains' rims. Zircons separated from this sample contain 279-2642 ppm U, 222-7281 ppm Th and Th/U = 0.7-3.5. We analyzed 35 zircon grains (Table S3A). Zircons are concordant or near concordant (Fig. 5) and yield a mean $^{206}Pb/^{238}U$ age of 536.8 ± 2.4 Ma (MSWD = 1.9). This is taken as the crystallization age of this hornblende-bearing metagabbro. Sample SH16-17 has zircon εHf values ranging from +6.5 to −7.9, more variable than the εHf values of other gabbroic zircons. Corresponding T_{DM}^C for zircons from sample SH16-17 vary from ~1.1 to 2 Ga.

4.3.4. Sample SH16-42

This sample is a highly deformed mylonitic metagabbro. It contains relict amphibole, plagioclase, clinopyroxene, with quartz and garnet. There are neither inherited cores nor metamorphic rims in zircon grains of this sample. Zircons are short-medium prismatic ~70-100 µm long. Most zircons display some oscillatory zoning.

The zircons contain 422-2833 ppm U, 277-4289 ppm Th and Th/U = 0.6-1.5. We analyzed 23 zircon grains from this sample (Table S3A). Nineteen analyses yield a mean $^{206}Pb/^{238}U$ age of 531.9 ± 2.4 Ma (MSWD = 1.6) (Fig. 5). This is taken as the crystallization age of this gabbroic rock. Zircons from sample SH16-42 displays a narrow range of εHf, between +3.1 and −0.1 (Table S5). Corresponding T_{DM}^C for zircons from sample SH16-42 vary from 1.5 to 1.3 Ga.

4.3.5. Sample SH16-34

This sample is taken from Torud gabbronorites and contain olivine, Cpx, Opx and plagioclase. Zircon grains from this sample are small, from ~50 µm. Most crystals have magmatic zonation. Twenty-four analyses are characterized by relatively moderate Th/U (~0.2-6.2) and low common lead (f_{206}, the proportion of common ^{206}Pb in total measured ^{206}Pb, <1.3%) (Table S3B). All analyses are concordant within analytical errors (Fig. 5), yielding a concordia age of 541.8 ± 2.9 Ma on a $^{206}Pb/^{238}U$ *vs* $^{207}Pb/^{235}U$ diagram. The weighted mean $^{206}Pb/^{238}U$ age of is 541.6 ± 3.3 Ma. This age is interpreted as the crystallization age of this sample. Zircon εHf values vary between +8.3 and −1.6 (Table S5). Corresponding T_{DM}^C for zircons from sample SH16-34 vary from 0.9 to 1.6 Ga.

4.3.6. Sample SH16-10

This sample is a tonalitic gneiss and contains plagioclase, amphibole and quartz with rare K-feldspar. Zircons are long prismatic (100-150 µm) and stubby with concentric and oscillatory zoning. Thirteen analyzed points show low Th/U of 0.2-0.6. Common lead (f_{206}) is <0.6%. The analyzed zircons give a weighted mean $^{206}Pb/^{238}U$ age of 542.1 ± 2.9 Ma (MSWD = 0.9). Zircons from sample SH16-10 display a narrow range of εHf, between −2.6 and −6.1 (Table S5). Crustal model ages for zircons from sample SH16-10 vary from 1.7 to 1.8 Ga.

4.3.7. Samples CHJ10-17, BJ11-26 and BJ11-27

These samples are taken from middle-crustal granodioritic gneisses and contain plagioclase, K-feldspar and quartz along with biotite and garnet. Zircons are mostly short to long-prismatic (>70 µm to 150 µm) and some have inherited cores. The analyzed spots (30 spots for each sample) have Th/U ratios of 0.1 to 0.6 with quite low common lead (nearly all zircons have $f_{206} < 1.9$).

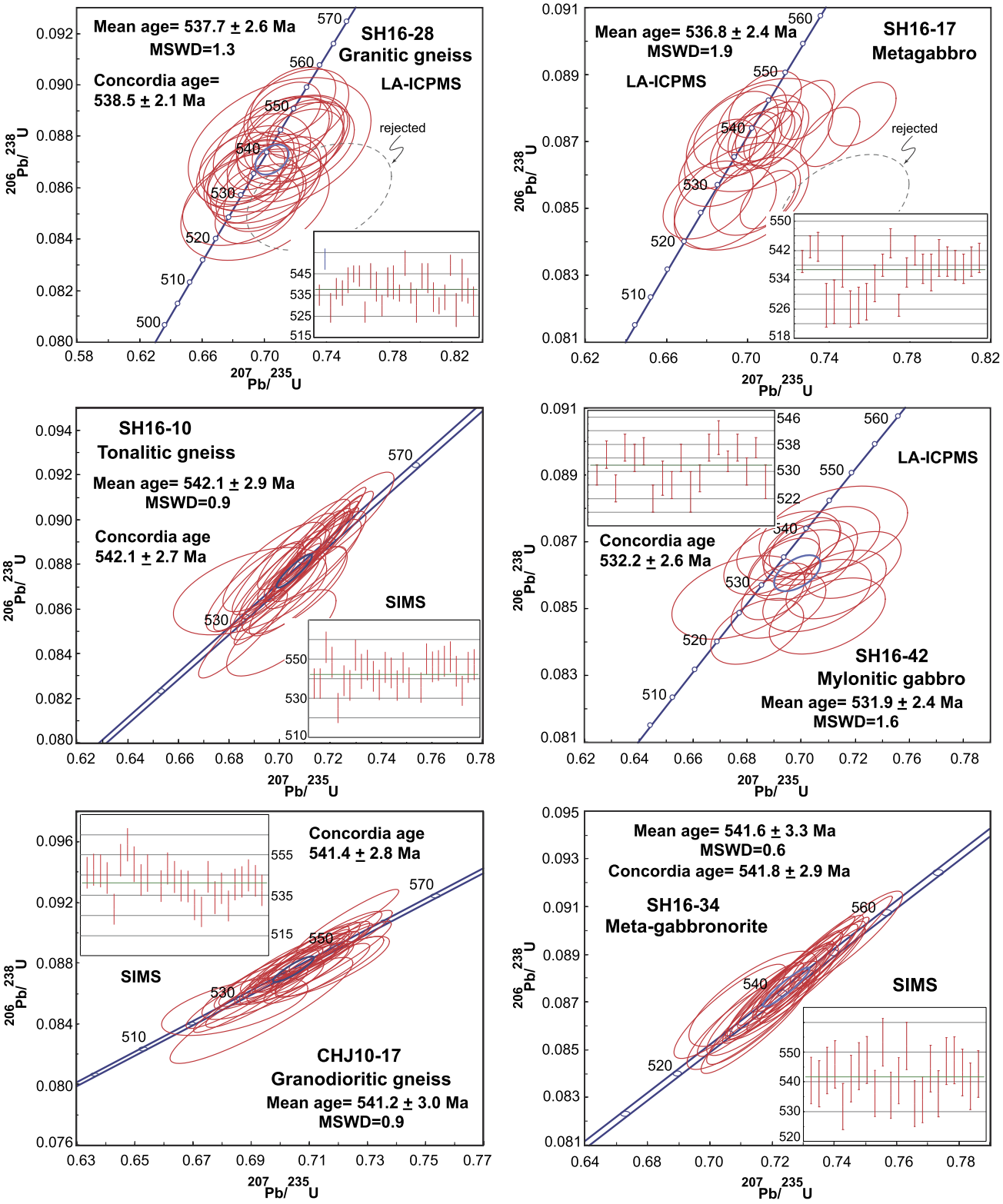

Fig. 5. Representative U-Pb concordia and mean $^{206}Pb/^{238}U$ age plots for the Cadomian metagabbros, mylonitic gabbros, meta-gabbronorites and tonalitic to granitic gneisses from NE Iran. The mean square of weighted deviates (MSWD) values are typically near (or less than) 1.0 (Max. < 2), indicating that the observed scatter in the data can be attributed to the assigned errors defined by analytical uncertainties (Ludwig, 2003).

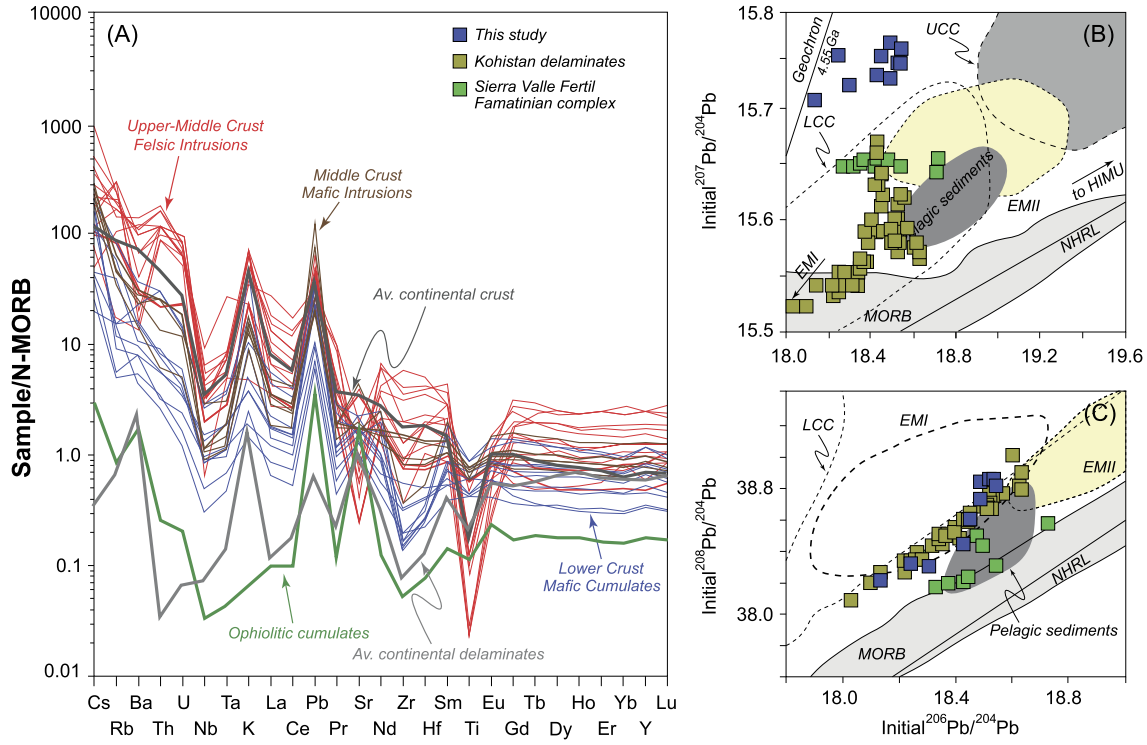

Fig. 6. A - Trace-element patterns of Cadomian upper-middle crust (felsic intrusions), middle crust (mafic intrusions) and lower crust (mafic cumulates) normalized to N-MORB. For comparison we have plotted average continental crust (Rudnick and Gao, 2003), average continental delaminates (Jagoutz and Schmidt, 2013) and (NE Iran) ophiolitic cumulates (Moghadam et al., 2014). B - $^{207}Pb/^{204}Pb$ *vs* $^{206}Pb/^{204}Pb$ and C - $^{208}Pb/^{204}Pb$ *vs* $^{206}Pb/^{204}Pb$ diagrams for Torud cumulate rocks. The Pb composition of pelagic sediments and continental upper and lower crust are from Plank and Langmuir (1998) and Rudnick and Gao (2003), respectively. The Pb composition of Kohistan and Famatinian arc delaminates are from Jagoutz and Schmidt (2012) and Walker et al. (2015), respectively.

Analyzed zircons are concordant within analytical errors (Figs. 5-S3) and yield weighted mean $^{206}Pb/^{238}U$ ages of 541.2 ± 3.0 Ma (MSWD = 0.9) for sample CHJ10-17, 545.2 ± 3.9 Ma (MSWD = 1.6) for sample BJ11-26 and 547.1 ± 3.2 Ma (MSWD = 0.9) for sample BJ11-27. Some other zircons show $^{206}Pb/^{238}U$ ages from >560 Ma up to 1 Ga and are considered to be inherited. Zircon εHf values for granodioritic gneisses range from +2.1 to −13.8, but most zircons show negative εHf ($av = -3.4$). Corresponding T_{DM}^{C} for these zircons vary from 1.4 to 2.3 Ga.

4.3.8. Sample CHJ10-33

This sample is taken from a granitic dike within the granodioritic gneisses. The sample is metamorphosed and contains K-feldspar, quartz, plagioclase, garnet, biotite and muscovite. Zircons from this sample are large (~100-150 μm) prismatic. Thirty analyzed spots have Th/U ratios between 0.2 and 0.7 (except one spot with Th/U = 0.01). Common-lead contents are low in most grains; with $f_{206} < 0.1\%$. The analyzed zircons yield a weighted mean $^{206}Pb/^{238}U$ age of 541 ± 3.2 Ma (MSWD = 0.6). This age is interpreted as the timing of dike crystallization. One inherited core shows a $^{206}Pb/^{238}U$ age of ~1 Ga. Zircon εHf values for this granitic dike vary between +1.1 and −7.7, with T_{DM}^{C} = 1.4-1.9 Ga.

4.3.9. Sample BJ11-19

This is a granitic gneiss and contains K-feldspar, quartz and minor plagioclase. Zircons from this sample are coarse-grained (~150 μm). Twenty-seven SIMS analyses were obtained. The zircons show a weighted mean $^{206}Pb/^{238}U$ age of 544.6 ± 3.5 Ma (MSWD=1.2). Zircon εHf values vary between +0.5 and −6.7, with T_{DM}^{C} = 1.5-1.9 Ga.

4.4. Thermobarometry

The Ti-in-zircon thermometer (Watson et al., 2006) yields temperatures of 849-815 °C for gabbros, 786 °C for mylonitic gabbros, 781 °C for metagabbros and 684 °C for granitic gneisses. These temperatures are lower than those calculated using the Fe-Mg ratios (K_D) of two equilibrated pyroxenes in gabbronorites (sample SH16-9; 1025 °C) or the Ca-in-Opx thermometer (1236 °C) (Brey and Köhler, 1990). The pressure calculated from amphibole geochemistry using the barometers of Hammarstrom and Zen (1986) and Schmidt (1992) is 8 kbar for metagabbros, 7.5 for gabbronorites and 5.7 kbar for gabbros, corresponding to depths of ~26 km, 25 km, and 19 km, respectively. A geothermal gradient of 30-45 °C/km has been calculated from these data.

4.5. Cumulate geochemistry

The Cadomian cumulates of NE Iran have low to moderate Mg# (29-50) with 46 to 55 wt% SiO_2 and 13.2 to 17.3 wt% Al_2O_3. TiO_2 contents are low; 0.5-1.1 wt%. These rocks are quite enriched in light-rare earth elements (LREEs) ($La_{(n)}/Yb_{(n)}$ = 1.9-7.8, normalized to N-MORB). The rocks are also enriched in incompatible elements such as Cs, Rb, Ba, Th, U, K and Pb but are depleted in Nb, Ta and Zr relative to the LREE, as is typical for arc-related igneous rocks (Fig. 6A). Mid-crustal felsic intrusions have high SiO_2 (74.1-76.5 wt%) but lower MgO (0.1-0.4) and Al_2O_3 (12.4-13). These rocks are enriched in LREEs with $La_{(n)}/Yb_{(n)}$ = 8.3-34.9. Positive anomalies in Cs, Rb, Ba, Th, U, K and Pb and depletion in Nb-Ta and Ti are conspicuous (Fig. 6A).

Cumulate rocks analyzed for Sr-Nd and Pb isotopes have variable initial $^{87}Sr/^{86}Sr_{(t)}$ (0.703-0.709) and εNd(t) values (−1.3 to +3.4). Initial $^{206}Pb/^{204}Pb_{(t)}$ and $^{208}Pb/^{204}Pb_{(t)}$ isotope ratios for these rocks vary from 18.14 to 18.55 and 38.21 to 38.85, respectively. $^{208}Pb/^{204}Pb_{(t)}$ ratios for these rocks are similar to pelagic

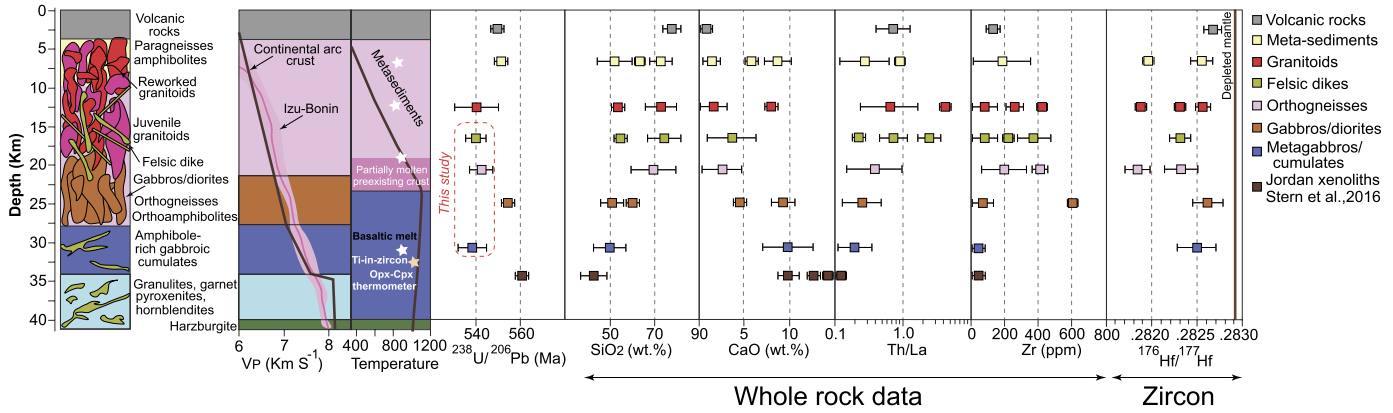

Fig. 7. Schematic illustrations of lithological, geochronological, seismic, temperature and geochemical-isotopic evolution of the NE Iran Cadomian arc section. The calculated average continental and oceanic seismic V_P velocities and temperature are from Jagoutz and Behn (2013). The thickness of the individual units is approximate. Ti-in-zircon (Watson et al., 2006) and Cpx-Opx thermometry results are shown for comparison. Data for Jordanian crustal xenoliths are from Stern et al. (2016).

limestones, whereas the $^{207}Pb/^{204}Pb_{(t)}$ ratios for cumulates are high (15.71 to 15.76) and are similar to upper continental crust (Fig. 6B-C).

5. Discussion

There are five main questions concerning NE Iran Cadomian cumulates and associated rocks. First, what is the timescale of magmatic buildup in the Cadomian crust of NE Iran? Second, did these cumulates form in a Cadomian deep crustal hot zone? Third, did differentiation (or assimilation-fractional crystallization = AFC) generate the middle-upper crust felsic rocks? Fourth, what caused the intense deformation in some of these rocks? Finally, what was the relationship between the deep crustal hot zone and the Cadomian magmatic flare-up? These questions are addressed below.

5.1. Repeated magmatic buildup

The summary of new zircon U-Pb age data shows gabbro cumulates have mean zircon $^{206}Pb/^{238}U$ ages of 542 ± 2.5 to 534 ± 2.1 Ma whereas a mylonitic gabbro has an age of 532 ± 2.4 Ma. Gabbronorites have mean $^{206}Pb/^{238}U$ ages of 542 ± 3.3 Ma, suggesting that mafic magmatism continued at least from ~542 ± 3.3 to 532±2.4 Ma (~10 ± 0.2 Myr). Mid-crustal intermediate to felsic intrusions and felsic dikes have mean $^{206}Pb/^{238}U$ ages of 547±3.2 to 538 ± 2.6 Ma (~9 ± 0.1 Myr). Mid-crustal intrusions have older ages of ~547 ± 3.2 Ma, but their ages (with uncertainties) also overlap with the crystallization of mafic cumulates (Fig. 7). This implies that younger mafic inputs were occurring while the more evolved portions of the middle crust of the arc were being established. These new data also indicate that the arc crust was constructed by magmatic buildup over a ~15 ± 0.3 Myr time scale. However, previously-published zircon U-Pb data on the middle-upper crustal intrusions and metasediments show ages of 561±4.2 to 530 ± 2.3 Ma, indicating a much longer magmatism (~31 ± 1 Myr). In addition, zircon U-Pb data attest that the Cadomian magmatism in Iran and Anatolia start at ~620 Ma and ended at 500 Ma. However, this ~120 Myr magmatic ignition seems to be spatially variable across different Cadomian arc segments in Iran and Anatolia. Continentally retreating arcs usually have an average lifespan of ~100 Myr, while oceanic arcs live for ~40 Myr (Ducea et al., 2015a). Extensional arcs such as the Cadomian arcs seem to be active for quite a bit longer (~120 Myr).

Cadomian magmatic pulses from NE Iran seem to have different Hf-isotopic compositions. The initial $^{176}Hf/^{177}Hf$ ratio of zircon from metagabbros ranges from $\varepsilon Hf(t) = -7.9$ to $+9.2$ ($av = +3.6$); a younger gabbro (sample SH16-43; 534 Ma) has more radiogenic Hf than the older gabbro sample (542 Ma). Sample SH16-17 has zircons with variable, but less radiogenic Hf isotopic compositions ($\varepsilon Hf(t) = -7.9$ to $+6.5$). Zircons from middle crust intrusions and dikes have variable $\varepsilon Hf(t)$ of -27.7 to $+5.4$ ($av = -4$). New zircon Lu-Hf isotope data highlight that middle crust felsic intrusions have less radiogenic Hf than deep gabbro cumulates.

5.2. Crustal profile and deep "hot zone"

In the "deep crustal hot zone" model, mantle-derived hydrous basaltic magmas are emplaced into the lower crust over a few million years as a succession of sills (Annen et al., 2006). Crustal "hot zones" are regions where MASH processes occur; they have been recognized in both continental arcs with thick crust (e.g., Andes, Annen et al., 2006) and intra-oceanic arcs with thin crust (e.g., Izu-Bonin-Mariana, Stern et al., 2019).

Partial crystallization of basaltic melts in the deep hot zones and interaction with surrounding rocks generates residual and anatectic H_2O-rich melts. These H_2O-rich melts and the heat released from the crystallizing magmas in turn promote partial melting of the adjacent pre-existing continental crust. Mixing of the H_2O-rich residual melts, primitive melts, and crustal melts leads to the diverse chemical and isotopic compositions of the resultant secondary magmas.

Cadomian igneous rocks formed along an active continental margin, with high fluxes of magmatism ("flare-up") in Ediacaran time (Moghadam et al., 2017d). Above this Neoproterozoic subduction zone, melting in the mantle wedge produced mafic magmas, which rose and stalled in the lower crust. The primary mantle melt that formed the Cadomian lower-crustal cumulates seems to have been a magnesian andesite (gabbronorite) because it crystallized both olivine and orthopyroxene. This melt had moderately low pH_2O, so that it first crystallized anhydrous phases (olivine and Opx) and plagioclase with quite low anorthite contents. Only later did water contents become high enough to crystallize amphibole.

Incomplete differentiation of these early, high-Mg phases in a deep-arc crustal hot zone produced silica-rich residual melts, which in turn fractionated in shallower magma chambers and assimilated older continental crust, to produce the granitoids that dominate the upper crust. Such shallow magma chambers solidified to form syn-tectonic granitoids and granitoid gneisses at depth and undeformed plutons at higher levels. Consistent with this overall scenario, lower-crustal rocks also have more juvenile zircon Hf (and whole rock Nd) isotope signatures than do shallower, more evolved igneous rocks. The middle-upper crustal rocks are affected by greater assimilation of pre-existing country

rocks, whereas mafic rocks show a relatively minor contribution of crustal components. The crustal isotopic (bulk rock Nd-Pb and zircon Hf) signature of the NE Iran gabbroic rocks can plausibly be attributed in part to a "contaminated" mantle source, in which the lithospheric mantle was already contaminated by crustal materials; either by lower crustal delamination or by subduction erosion (Lackey et al., 2005).

Fig. 7 shows that bulk rock SiO_2 and Zr increase from lower-crustal cumulates to upper-crustal intrusions, whereas CaO decreases, showing the importance of fractionation of early-crystallized minerals for magmatic evolution. Plots of trace elements on a N-MORB normalized diagram (Fig. 6) indicate that magmatic fractionation dominated, leading to major negative anomalies in some elements such as Ti and enrichment in other incompatible elements such as Zr and HREEs in fractionated middle-upper crustal rocks compared with the lower-crustal cumulates. The range of zircon Hf and bulk rock Nd isotopic compositions suggest thats AFC was also important. We infer that a hot zone in the middle and lower crust was responsible for forming the more evolved magmas that now comprise the rocks of the Cadomian middle to upper crust of NE Iran.

A crustal profile of the Cadomian arc of Iran has been reconstructed by using Sr/Y elemental ratios for intermediate rocks (Chapman et al., 2015; Chiaradia, 2015) and Ce/Y ratios for mafic rocks (Mantle and Collins, 2008). Chapman et al. (2015) suggested that Sr/Y can be used as a proxy for crustal thickness in intermediate calc-alkaline rocks (55-68 wt% SiO_2). Our compiled data show that most Cadomian rocks with intermediate SiO_2 reflect a crustal thickness of 20 to 30 km. Gabbroic cumulates (*this study*) have maximum Ce/Y ratios <1.4, indicating a crustal thickness for the Iran Cadomian arc of <30 km. However, considering the Sr can be affected by plagioclase fractionation, we have also used the Gd/Yb and La/Yb ratios (which are sensitive to garnet fractionation) for our intermediate rocks (55-68% SiO_2) (Farner and Lee, 2017). These results also confirm a thin crustal profile (20-30 km) for the Cadomian crust of Iran. Al-in-amphibole geobarometry also records an emplacement depth of 19-26 km for the metagabbros, just above the Cadomian Moho beneath NE Iran.

5.3. FC-AFC processes and generation of the Cadomian arc crust

Rayleigh Fractional crystallization (FC) and coupled Assimilation-Fractional Crystallization (AFC) models can be used to test the hypothesis that Cadomian magmatic rocks are cogenetic melts, belonging to a common line of descent, with middle-upper crust felsic rocks derived through progressive differentiation starting from the same mafic parental melt. Based on mineral- and whole rock chemistry, a gabbronorite (sample SH16-9) and a hornblende-bearing metagabbro (sample SH16-17) were selected as best approximations to parental magma compositions. Eighty-four FC-models were developed in order to test the working hypothesis.

Major-element mass-balance models show that the studied gabbroic rocks (SiO_2 < 52 wt%, lower and middle crust mafic intrusions) reflect 30-67% fractional crystallization of gabbronoritic parental melts with a crystallizing assemblage of clinopyroxene, plagioclase, olivine and ilmenite ($Cpx_{2.3\text{-}13.3}$ + $Pl_{26.5\text{-}40.8}$ + $Ol_{49.4\text{-}59.9}$ + $Ilm_{<2}$; hereafter percentages are given for the total crystallized assemblage). Approximately 75-92% fractional crystallization of a similar assemblage ($Cpx_{11.7\text{-}14.2}$ + $Pl_{41.5\text{-}42.3}$ + $Ol_{41.5\text{-}54.9}$ + $Ilm_{<2}$), can produce higher-silica (SiO_2 > 52 wt%) lower and middle crust mafic intrusions (metagabbros, gabbros and diorites) from the same gabbronoritic (SH16-9) parental melt. Moreover, differentiation of gabbronoritic melt to form middle and upper crust felsic rocks can result from 91-94% fractional crystallization of the previous assemblage ($Cpx_{13\text{-}16.3}$ + $Pl_{40.1\text{-}43.0}$ + $Ol_{41.1\text{-}42.2}$ + $Ilm_{1.8\text{-}2.2}$). However, these fractionating assemblages fail to perfectly reproduce all upper crust felsic rocks (granites and rhyolites) and the overall differentiation trend (Σr^2 *ca* 0.9-1.0), mainly due to the large r^2 for Ti, Fe, Mg and Ca, suggesting either the presence of another concurrent fractionating assemblage, or assimilation of crustal felsic material. Crustal assimilation is also indicated by the variable isotopic signatures of the rocks.

Given the presence of Ca-amphibole in the gabbroic rocks, mass balance models have been recalculated for an assemblage with hornblende (Cpx + Pl + Hbl + Ilm). Model solutions show that Cadomian intermediate and felsic rocks (SiO_2 > 54 wt%) could be the result of 72-85% fractional crystallization of Hbl gabbros (sample SH16-17) with an assemblage of clinopyroxene, plagioclase, hornblende and ilmenite ($Cpx_{0\text{-}5.4}$ + $Pl_{12.1\text{-}24.3}$ + $Hbl_{66.8\text{-}86.3}$ + $Ilm_{1.8\text{-}2.1}$). Even if the hornblende-bearing assemblage is more efficient in producing upper-crustal rhyolites, these mass balance models again fail to reproduce the compositions of the middle and upper crust felsic intrusions (Σr^2 *ca* 0.9-1.0) due to the large r^2 for Fe, Mg and K. Results from FC-models thus again suggest that crustal assimilation of silica-rich/felsic materials was coupled to fractional crystallization processes (e.g. McBirney et al., 1987) to produce the high-SiO_2 melts (granites and rhyolites) of the Cadomian upper crust.

A Harker-like plot for major element mass-balance FC and AFC models is presented in Fig. 7. FC trends are reported for three representative fractionating assemblages (see Appendix B): i) *Ol1* ($Cpx_{2.6}$ + $Pl_{40.8}$ + $Ol_{54.9}$ + $Ilm_{1.6}$), ii) *Ol2* ($Cpx_{14.0}$ + $Pl_{42.6}$ + $Ol_{41.3}$ + $Ilm_{2.1}$) and iii) *Hbl* ($Cpx_{3.0}$ + $Pl_{20.8}$+ $Hbl_{74.5}$ + $Ilm_{1.7}$).

In order to verify mass-addition phenomena in the genesis of high-SiO_2 Cadomian felsic melts (i.e., granites and rhyolites), we tested AFC models based on the interaction between the gabbroic parental melts and a high-SiO_2 Cadomian upper crust felsic sediment (the BJ10-32 paragneiss sample). AFC curves (Fig. 8) calculated through the lever-rule methods represent the maximum assimilation (mass-addition) effect, whereas the null value is represented by the pure FC curves. The compositional space between the AFC and the FC curves, indicates fractionated/residual liquids generated by coupled FC and AFC processes. The results (Fig. 8) indicate that assimilation of silica-rich sediments played a dominant role in the production of the most felsic Cadomian upper crust melts.

Based on the major-element FC-AFC solutions, we applied FC-AFC models to selected trace elements (La, Yb, Nb and Y) to further investigate the major role of fractionating assemblages such as Ca-plagioclase, Ca-hornblende and Mg-olivine (Fig. 9). The results obtained from these models are consistent with those based on major-element models and further support the general hypothesis that FC-AFC processes controlled the Cadomian magmatism. FC-models calculated for olivine-bearing assemblages (Ol1 and Ol2) suggest that the lower- and middle-crustal mafic intrusions (i.e. gabbros and metagabbros) were produced by 40-60% fractional crystallization of the parental melts.

FC-curves (maximum and minimum) calculated for both olivine-(Ol1 and Ol2) and hornblende-bearing (Hbl) assemblages indicate that most granitoid rocks (upper- to middle-crust felsic intrusions) are not the products of pure fractional crystallization from a mafic parental melt (neither gabbronorite nor hbl-metagabbro). However, a combination of fractional crystallization (FC 40-90%) and concurrent assimilation of ~20% (*proportion of assimilant to fractionates* = 0.2) of Cadomian upper-crustal SiO_2-rich sediments is required to produce most Cadomian felsic rocks.

FC-AFC models indicate that all Cadomian magmatic rocks are cogenetic and belong to a common line of descent. Thermobarometric estimates suggest magmatic differentiation, from parental gabbros to intermediate daughter melts, occurred in the lower crust at pressures between 5.7-8 kbar (*ca* 30-19 km), in agreement with the model proposed by Annen et al. (2006) for the gene-

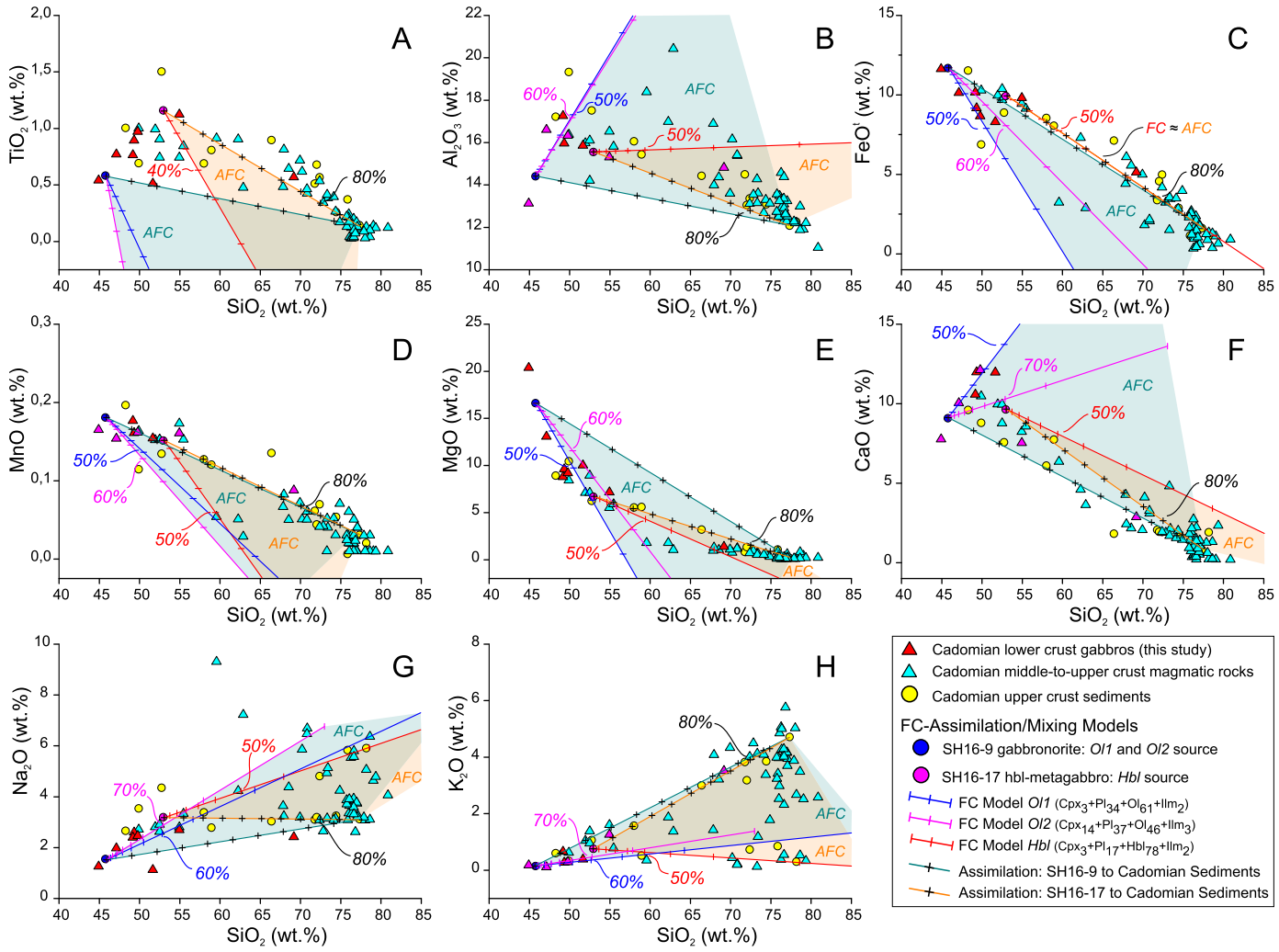

Fig. 8. Fractional crystallization (FC)/Assimilation-fractional crystallization (AFC) major element modeling of Cadomian magmatic rocks. Major elements have been recalculated to 100% anhydrous, in the system SiO_2-TiO_2-Al_2O_3-FeO*-MnO-MgO-CaO-Na_2O-K_2O. *Blue* and *pink circles* represent the suspected parental melts; SH16-9 and SH16-17, respectively. *Blue* and *pink lines* represent olivine-1 (Ol1) and olivine-2 (Ol2) fractionation trends respectively, as calculated for SH16-9 gabbronoritic melt. *Red line* represents hornblende (Hbl) fractionation trend as calculated for SH16-17 metagabbroic melt. *Green* and *orange lines* represent maximum assimilation trends as calculated for the suspected parental gabbronoritic and Hbl-metagabbroic melts, respectively. The domains of possible AFC processes are presented in *green* and *orange shaded areas* (for gabbronorite SH16-9 and metagabbro SH16-17, respectively) situated between maximum assimilation/mixing- and FC-trends. Silica poor/mafic upper crust metamorphosed sediments are equivalents of greywackes and tuffaceous sediments.

sis of intermediate and silicic magmas in deep crustal hot zones. The non-unique nature of FC-models implies, in these deep crustal hot zones, the presence of distinct MASH-zones (e.g., Annen et al., 2006; Ginibre and Worner, 2007 where different fractionating assemblages (olivine *vs* hornblende) reflect the polybaric conditions of the magmatic system (e.g., Ginibre and Worner, 2007). Moreover, U-Pb zircon ages reveal a prolonged magmatic activity that lasted *ca* 45 Myr, and together with the results obtained from FC-AFC models, strongly support the hypothesis of the buildup of a deep mafic reservoir progressively feeding the shallower magmatic systems (Ginibre and Worner, 2007).

However, a long-lived magmatic flare-up and the buildup of a deep crustal hot zone require a continuous upload and recharge of parental magma from the source to sustain the whole magmatic system. Without magmatic recharge, in a closed system controlled by solely FC-processes, the mass of the residual/daughter liquids will progressively decrease (e.g., Albarède, 1996; Lee et al., 2014), and all melt will crystallize and cool due to the interaction with the cold country rocks (Lee et al., 2014). On the other hand, a continuous replenishment of magma in the magmatic plumbing system (a) will decrease cooling and crystallization rates, (b) will sustain the mass of evolving residual liquids and (c) will trigger melt evacuation and ascent through the crust (e.g., Depaolo, 1981; Ginibre and Worner, 2007; Lee et al., 2014). Existing numerical models (e.g., Karlstrom et al., 2010) indicate that for a given recharge rate, deep crustal magmatic reservoirs are less prone to evacuate/erupt melts than shallower magmatic stagnation layers where (a) recharge effects are less significant and (b) eruption and cooling are more efficient due to lower confining pressure and colder country rocks (e.g., Lee et al., 2014 and references therein). In the deep crustal mafic reservoir, the lower evacuation rate will progressively produce growing recharging chambers by deforming the hot lower crust wall-rocks (Jellinek and DePaolo, 2003; Karlstrom et al., 2010; Lee et al., 2014).

This scenario supports the presence of a Cadomian deep crustal hot zone where long-lived mafic magma chambers mature and expand due to a higher recharge rate with respect to the mass of the magma reservoir. This long-lived Cadomian mafic reservoir is then interpreted as the parental source of nearly all Cadomian magmatic rocks of Iran produced via general FC-AFC processes evolving in the crust.

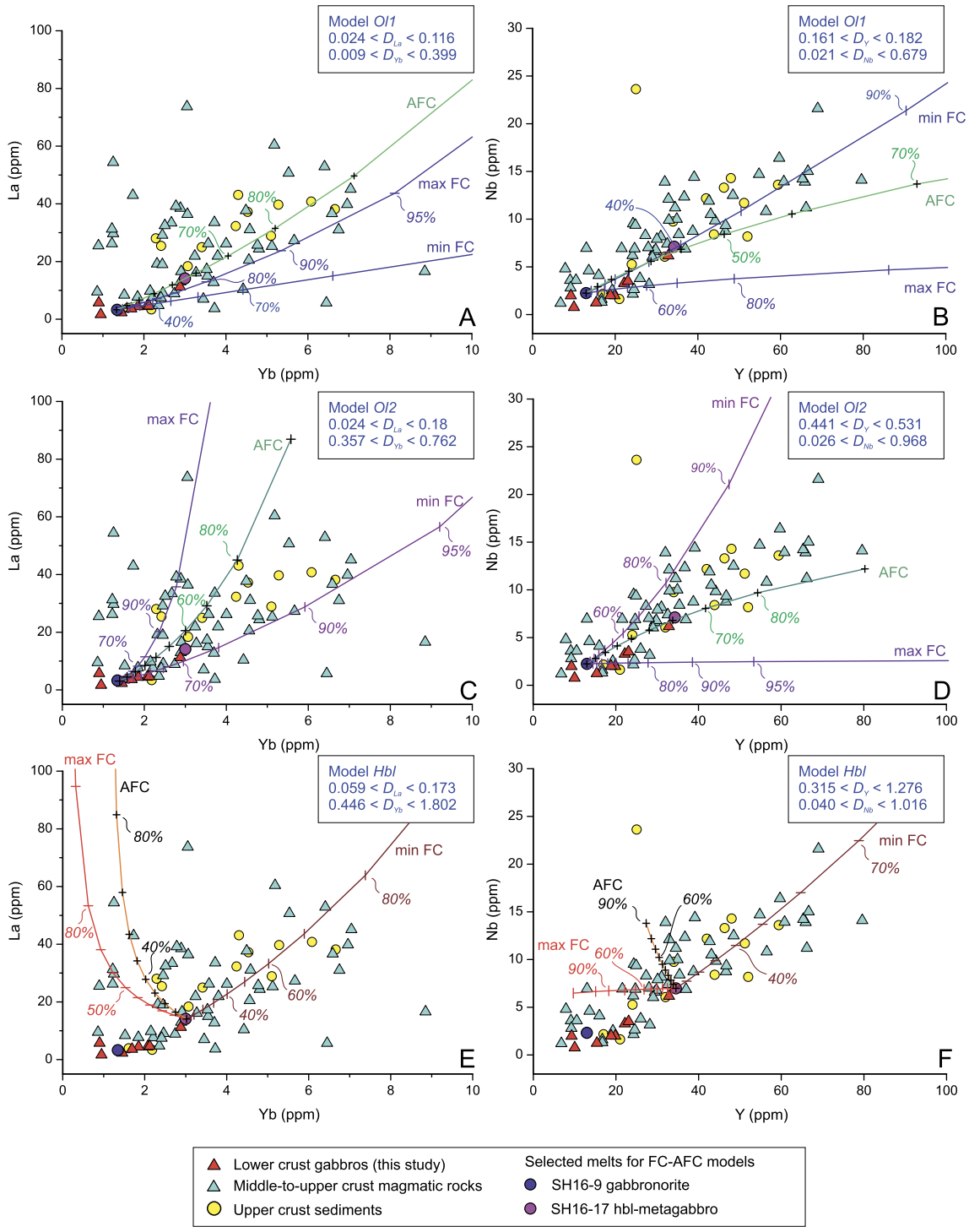

Fig. 9. La *vs* Yb and Nb *vs* Y diagrams illustrating the genesis of the Cadomian magmatic suite via FC-AFC of olivine (Ol1 and Ol2) and hornblende (Hbl) assemblages, starting from parental gabbroic samples SH16-9 and SH16-17, respectively. Bulk rock/melt partition coefficient used are reported in diagrams and were calculated following the procedure presented in section 4.4 in Appendix B. FC-curves represent, for every model, Rayleigh fractional crystallization solutions calculated for minimum K_D (min FC) and for maximum K_D (max FC) values. AFC-curves represent De Paolo Assimilation and fractional crystallization solutions. The percentages indicate amount of fractionating assemblages. Equations and parameters used are presented in Appendix B.

5.4. Deep arc crust and deformation

The above calculations imply that the Cadomian flare-up magmatism must have generated a dense root of ultramafic-mafic cumulates, 3-4 times as voluminous as the present Iranian crust. There is no evidence for the presence of such a thick root beneath Iran today, and it may have foundered into the mantle (Ducea, 2002), perhaps even during the magmatic flare-up, when the lower crust is hottest and weakest and the largest volumes of dense cumulates are produced. The preservation of thick cumulates in the lower crust of arcs is unusual, as they commonly either delaminate after the flare-up event or are tectonically removed during the later plate tectonic movements (Chapman et al., 2016). Garnet-rich cumulates are especially dense and prone to sinking, and it is likely that the shallow limit of garnet stability (~30 km) made it impossible to thicken the Iran-Anatolia Cadomian crust beyond this.

Besides the missing volume of mafic-ultramafic cumulates, there may be other evidence of Cadomian lower-crustal foundering. The occurrence of metamorphic coronas between olivine and plagioclase with fine-grained vermicular garnet crystals and the presence of garnet in mylonitic gabbros attest to a phase of high-grade metamorphism and intense deformation that may have occurred during foundering of cumulates. Most coronas between olivine and plagioclase contain layers of orthopyroxene and amphibole ± spinel suggesting partial re-equilibration in the presence of a fluid-rich phase (Otamendi et al., 2010), but in more complex cases garnet is seen near reactant plagioclase.

The EBSD-derived images from mylonitic gabbros also hint at deformation of early-crystallized clinopyroxenes and coarse-grained amphiboles. In the mylonitic gabbro (sample SH16-42), the crystal preferred orientation (CPO) of amphibole and Cpx show similar direction for the [001] (i.e. [001] cluster with an m.u.d above 3) and [010] axes. These, together with the close textural relationship between the two minerals (Fig. 4), may suggest that the coarse-grained amphiboles grew epitaxially on the pre-existing Cpx (as seen in other fields; e.g., Henry et al., 2017; Puelles et al., 2012). The significant amount of misorientation in both Cpx and coarse-grained amphibole suggests that they both record a plastic deformation episode. This deformation likely occurred after the growth of the coarse-grained amphibole and could be responsible of the second cluster of [001] axes of amphibole which is at a high angle to that of the Cpx. The presence of abundant, equilibrated and relatively fine-grained amphibole suggests partial annealing of the texture, thus hinting at a significant weakening of the stress field in the later history of the sample.

The occurrence of deformed amphibole associated with clinopyroxene relics may indicate protracted polybaric crystallization involving a second H_2O-rich melt ($H_2O > 4$ wt%), which was cool enough (<1000 °C) to stabilize amphibole (Muntener et al., 2001). This seems to have happened deep in the arc crust, as indicated by the high Al_2O_3 content and strong deformation of the pargasitic amphiboles. All these textural and microstructural evidences as well as P-T conditions are compatible with deformation and metamorphism in the deep crust, perhaps accompanying the foundering of the lower crust. Middle-upper crustal felsic intrusions also show evidence of plastic deformation suggesting a crust-wide tectonic activity.

5.5. Tempos of Cadomian arc magmatism

The Cadomian arcs of Iran-Anatolia were important sites of continental growth, with the bulk of igneous rocks being emplaced during the Ediacaran flare-up. This magmatic flare-up was responsible for forming ~30 km of Cadomian crust in Iran-Anatolia, consisting of gabbroic cumulates, variably metamorphosed mafic to felsic intrusions and felsic volcanic-pyroclastic rocks (Fig. 10A). The existence of mafic and felsic magmatic rocks among the Cadomian outcrops indicates bimodal magmatic activity (Fig. 10), which is well known from modern intra-oceanic and Andean-type arcs (e.g., Ducea et al., 2015a; Stern et al., 2014). Some estimate that the generation of such large volumes of crust involves about 50% from melting of lower continental crust and lithospheric mantle and 50% from melting of the metasomatized mantle wedge above the subducting oceanic slab (DeCelles et al., 2009; Ducea et al., 2015a). Plutonism is the principle expression of magmatic flare-ups, with ratios of plutonism to volcanism estimated as high as ~30:1 (Paterson and Ducea, 2015). The Cadomian arcs of Iran-Anatolia (and perhaps Europe, SW Asia, and E. North America) record both abundant plutonism and significant volcanism accompanying crustal thickening and long-lived magmatism involving melting of both the mantle and overlying continental crust (Moghadam et al., 2017d). Although our new data on Cadomian crust of NE Iran indicate a ~15 ± 0.3 Myr of magmatic activity, our compiled zircon U-Pb data on the Cadomian magmatic rocks of Iran demonstrate an intense episode of magmatic activity that lasted ~45 Myr, from 570 to 525 Ma (Fig. 10B), involving magmas with different geochemical signatures and isotopic disturbances (Figs. 10F-G) (Moghadam et al., 2017d). The most obvious products of the Cadomian flare-up are the igneous rocks of the upper crust: felsic plutons and volcanics (Figs. 10C & E). In spite of this, it was mafic magmatism that powered the flare-up episode, and similar magmas also prevail during episodes of normal arc magmatism (Fig. 10D). There is no evidence for repeated flare-up episodes in SW Asia Cadomian arcs. The flare-ups may have halted when plate motions changed, leading to opening of a back-arc basin that grew into the Rheic Ocean. Uplift and erosion related to this supplied a thick sequence (>1000 m) of detrital sediments in Iran and Anatolia, derived predominantly (>90%) from erosion of Cadomian igneous rocks (Moghadam et al., 2017c).

The 40 Myr flare-up stage was characterized by an increase of magmatic flux rates by >3 orders of magnitude, compared to the "steady-state" flux, coupled with a significant disturbance in Sr-Nd-Hf isotope ratios (Figs. 10F-G) and a major contribution of pre-existing crustal rocks through AFC processes. The flare-up completely obliterated these older rocks; the only traces of their existence are found in the isotopic compositions of igneous rocks and in detrital zircons in sediments. In the Cadomian arcs of Iran and Anatolia, the inheritance ages are dominated by *ca* 1.3-1.4 and 2.5 Ga zircons (Moghadam et al., 2017d), which is consistent either with the presence of as-yet undiscovered older Gondwanan crust or recycling of sediments through the arc system. Influx of asthenospheric materials to the arc root, due to the foundering of dense cumulates, may trigger the generation of more mafic magmas. This process has been suggested to explain the isotopic disruption of magmatic rocks from other arcs (e.g., Paterson and Ducea, 2015; Stuart et al., 2016).

6. Conclusions

The Cadomian arcs of Iran and Anatolia are viewed as "Andean" because they were emplaced within an old craton, although their extensional behavior makes them different than Andean arcs. Our new zircon U-Pb ages indicate that the Cadomian arc crust of NE Iran was built over ~15 Myr, similar to some modern arcs. However, all compiled data from Cadomian exposures in Iran and Anatolia show magmatism started at 620 Ma and ended at ~500 Ma with a flare-up period for ~45 Myr (570-525 Ma). This shows that the magmatism was temporally and spatially different in various sections of the Cadomian arc. Cadomian arcs were intruded by voluminous mafic magmas that differentiated, generating intermediate melts that then interacted with variable amounts of middle-upper crust sediments to produce middle-upper crust felsic intrusions.

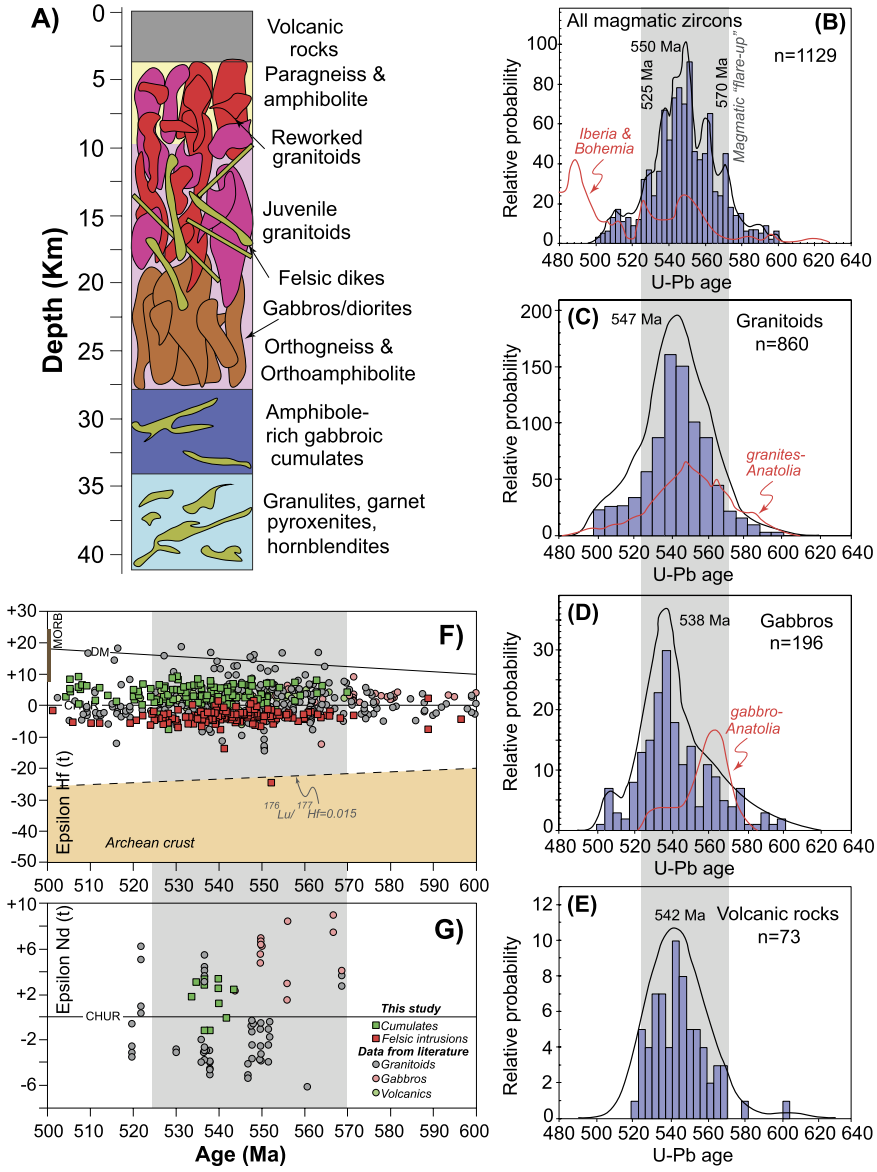

Fig. 10. A schematic crustal column through the Cadomian arc crust of Iran. (B-E) Histograms showing the magmatic age distribution of all Cadomian rocks (B), granitoids (C), gabbros (D) and volcanic rocks (E) from Iran. (F and G) Evolution plots of isotopic (bulk rock Nd and zircon Hf) geochemistry of Iran Cadomian igneous rocks. CHUR = chondrite normalized uniform reservoir; DM = depleted mantle array (based on data from modern Mid-Oceanic Ridge basalts with $^{176}Hf/^{177}Hf = 0.28325$ and using $^{176}Lu/^{177}Hf = 0.0384$ (Chauvel and Blichert-Toft, 2001)). Published zircon U-Pb-Hf and bulk rock Sr-Nd data from Iran are from Moghadam et al. (2017b, 2015, 2017d), data from Anatolia and Iberia are from Abbo et al. (2015), Gursu (2016), Ustaomer et al. (2012) and Pereira et al. (2012), respectively.

Our data show that the Cadomian magmatism in Iran and Anatolia was characterized by high rates of magmatic addition (>300 $km^3\ km^{-1}\ yr^{-1}$), which seems to be related to a phase of high arc migration rate across Prototethyan trench (or roll-back). This produced extreme extension in the overlying continental crust of the subduction system, resulting in a flare-up episode. Thick arcs, such as the Cadomian arc of Iran and Anatolia, are also characterized by the buildup of dense cumulates in the lower crust, which can drive the magmatic intensity into a lull period. Long-lived arcs or those which are under flare-up have higher mafic-ultramafic cumulates and thus thicker roots (>30 km).

Declaration of competing interest

The authors declare that they have no known competing financial interests or personal relationships that could have appeared to influence the work reported in this paper.

Acknowledgements

This study was funded by the "National Key Research and Development Program of China (2016YFE0203000, Q.L. Li)" and by "Chinese Academy of Sciences, President's International Fellowship Initiative (PIFI, 2019VCB0013, HSM)". This study used instrumentation funded by ARC LIEF and DEST Systemic Infrastructure Grants, Macquarie University, NCRIS AuScope and Industry. This is contribution 1381 from the ARC Centre of Excellence for Core to Crust Fluid Systems (http://www.ccfs.mq.edu.au) and 1330 in the GEMOC Key Centre (http://www.gemoc.mq.edu.au). The authors acknowledge the facilities, and the scientific and technical assistance of the Australian Microscopy & Microanalysis Research Facility at the Electron Microscope Unit, The University of New South Wales, Australia. We are very grateful to X.X. Ling, J. Li and Y.H. Yang (IGG-CAS) for their assistance during zircon SIMS dating and LA-MC-ICPMS Lu-Hf isotope analyses. We also thanks K. Pri-

vate for her assistance during EPMA. This paper benefited from discussion and advice from J.C. White. We are very grateful to E.J. Chin and an anonymous reviewer for their constructive reviews of the manuscript. Editorial suggestions by An Yin are appreciated. All logistical supports for the field work come from Damghan University.

Appendix. Supplementary material

Supplementary material related to this article can be found online at https://doi.org/10.1016/j.epsl.2019.115989.

References

Abbo, A., Avigad, D., Gerdes, A., Gungor, T., 2015. Cadomian basement and Paleozoic to Triassic siliciclastics of the Taurides (Karacahisar dome, south-central Turkey): paleogeographic constraints from U-Pb-Hf in zircons. Lithos 227, 122–139.

Albarède, F., 1996. Introduction to Geochemical Modeling. Cambridge University Press.

Annen, C., Blundy, J.D., Sparks, R.S.J., 2006. The genesis of intermediate and silicic magmas in deep crustal hot zones. J. Petrol. 47, 505–539.

Behn, M.D., Kelemen, P.B., 2006. Stability of arc lower crust: insights from the Talkeetna arc section, south central Alaska, and the seismic structure of modern arcs. J. Geophys. Res., Solid Earth 111.

Brey, G., Köhler, T., 1990. Geothermobarometry in four-phase lherzolites II. New thermobarometers, and practical assessment of existing thermobarometers. J. Petrol. 31, 1353–1378.

Chapman, J.B., Ducea, M.N., DeCelles, P.G., Profeta, L., 2015. Tracking changes in crustal thickness during orogenic evolution with Sr/Y: an example from the North American Cordillera. Geology 43, 919–922.

Chapman, T., Clarke, G., Daczko, N., 2016. Crustal differentiation in a thickened arc—evaluating depth dependences. J. Petrol. 57, 595–620.

Chauvel, C., Blichert-Toft, J., 2001. A hafnium isotope and trace element perspective on melting of the depleted mantle. Earth Planet. Sci. Lett. 190, 137–151.

Chiaradia, M., 2015. Crustal thickness control on Sr/Y signatures of recent arc magmas: an Earth scale perspective. Sci. Rep. 5.

Christensen, N.I., Mooney, W.D., 1995. Seismic velocity structure and composition of the continental crust: a global view. J. Geophys. Res., Solid Earth 100, 9761–9788.

DeCelles, P.G., Ducea, M.N., Kapp, P., Zandt, G., 2009. Cyclicity in Cordilleran orogenic systems. Nat. Geosci. 2, 251–257.

Depaolo, D.J., 1981. Trace element and isotopic effects of combined wallrock assimilation and fractional crystallization. Earth Planet. Sci. Lett. 53, 189–202.

Ducea, M.N., 2002. Constraints on the bulk composition and root foundering rates of continental arcs: a California arc perspective. J. Geophys. Res., Solid Earth 107.

Ducea, M.N., Bergantz, G.W., Crowley, J.L., Otamendi, J., 2017. Ultrafast magmatic buildup and diversification to produce continental crust during subduction. Geology 45, 235–238.

Ducea, M.N., Paterson, S.R., DeCelles, P.G., 2015a. High-volume magmatic events in subduction systems. Elements 11, 99–104.

Ducea, M.N., Saleeby, J.B., Bergantz, G., 2015b. The architecture, chemistry, and evolution of continental magmatic arcs. Annu. Rev. Earth Planet. Sci. 43 (43), 299–331.

Farner, M.J., Lee, C.-T.A., 2017. Effects of crustal thickness on magmatic differentiation in subduction zone volcanism: a global study. Earth Planet. Sci. Lett. 470, 96–107.

Ginibre, C., Worner, G., 2007. Variable parent magmas and recharge regimes of the Parinacota magma system (N. Chile) revealed by Fe, Mg and Sr zoning in plagioclase. Lithos 98, 118–140.

Gursu, S., 2016. A new petrogenetic model for meta-granitic rocks in the central and southern Menderes Massif – W Turkey: implications for Cadomian crustal evolution within the Pan-African mega-cycle. Precambrian Res. 275, 450–470.

Hammarstrom, J.M., Zen, E.-a., 1986. Aluminum in hornblende: an empirical igneous geobarometer. Am. Mineral. 71, 1297–1313.

Henry, H., Tilhac, R., Griffin, W.L., O'Reilly, S.Y., Satsukawa, T., Kaczmarek, M.-A., Grégoire, M., Ceuleneer, G., 2017. Deformation of mantle pyroxenites provides clues to geodynamic processes in subduction zones: case study of the Cabo Ortegal Complex, Spain. Earth Planet. Sci. Lett. 472, 174–185.

Hosseini, S.H., Sadeghian, M., Zhai, M.G., Ghasemi, H., 2015. Petrology, geochemistry and zircon U-Pb dating of Band-e-Hezarchah metabasites (NE Iran): an evidence for back-arc magmatism along the northern active margin of Gondwana. Chem. Erde 75, 207–218.

Jagoutz, O., 2014. Arc crustal differentiation mechanisms. Earth Planet. Sci. Lett. 396, 267–277.

Jagoutz, O., Behn, M.D., 2013. Foundering of lower island-arc crust as an explanation for the origin of the continental Moho. Nature 504, 131.

Jagoutz, O., Schmidt, M., 2013. The composition of the foundered complement to the continental crust and a re-evaluation of fluxes in arcs. Earth Planet. Sci. Lett. 371, 177–190.

Jagoutz, O., Schmidt, M.W., 2012. The formation and bulk composition of modern juvenile continental crust: the Kohistan arc. Chem. Geol. 298, 79–96.

Jellinek, A.M., DePaolo, D.J., 2003. A model for the origin of large silicic magma chambers: precursors of caldera-forming eruptions. Bull. Volcanol. 65, 363–381.

Jicha, B.R., Jagoutz, O., 2015. Magma production rates for intraoceanic arcs. Elements 11, 105–111.

Karlstrom, L., Dufek, J., Manga, M., 2010. Magma chamber stability in arc and continental crust. J. Volcanol. Geotherm. Res. 190, 249–270.

Kitamura, K., Ishikawa, M., Arima, M., 2003. Petrological model of the northern Izu-Bonin-Mariana arc crust: constraints from high-pressure measurements of elastic wave velocities of the Tanzawa plutonic rocks, central Japan. Tectonophysics 371, 213–221.

Lackey, J.S., Valley, J.W., Saleeby, J.B., 2005. Supracrustal input to magmas in the deep crust of Sierra Nevada batholith: evidence from high-delta O-18 zircon. Earth Planet. Sci. Lett. 235, 315–330.

Lee, C.T.A., Lee, T.C., Wu, C.T., 2014. Modeling the compositional evolution of recharging, evacuating, and fractionating (REFC) magma chambers: implications for differentiation of arc magmas. Geochim. Cosmochim. Acta 143, 8–22.

Linnemann, U., Romer, R.L., Gerdes, A., Jeffries, T.E., Drost, K., Ulrich, J., 2010. The Cadomian orogeny in the Saxo–Thuringian zone. In: Linnemann, U., Romer, R.L. (Eds.), Pre–Mesozoic Geology of Saxo–Thuringia – From the Cadomian Active Margin to the Variscan Orogen. Schweizerbart, Stuttgart, pp. 37–58.

Ludwig, K.R., 2003. User's manual for isoplot 3.00, a geochronlogical toolkit for Microsoft Excel. Berkeley Geochronl. Cent. Spec. Publ. 4, 25–32.

Malekpour-Alamdari, A., Axen, G., Heizler, M., Hassanzadeh, J., 2017. Large-magnitude continental extension in the northeastern Iranian Plateau: insight from K-feldspar $^{40}Ar/^{39}Ar$ thermochronology from the Shotor Kuh–Biarjmand metamorphic core complex. Geosphere 13, 1207–1233.

Mantle, G., Collins, W., 2008. Quantifying crustal thickness variations in evolving orogens: correlation between arc basalt composition and Moho depth. Geology 36, 87–90.

McBirney, A., Taylor, H., Armstrong, R., 1987. Paricutin re-examined: a classic example of crustal assimilation in calc-alkaline magma. Contrib. Mineral. Petrol. 95, 4–20.

Moghadam, H.S., Bröcker, M., Griffin, W.L., Li, X.H., Chen, R.X., O'Reilly, S.Y., 2017a. Subduction, high-P metamorphism, and collision fingerprints in South Iran: constraints from zircon U-Pb and mica Rb-Sr geochronology. Geochem. Geophys. Geosyst. 18, 306–332.

Moghadam, H.S., Corfu, F., Chiaradia, M., Stern, R.J., Ghorbani, G., 2014. Sabzevar Ophiolite, NE Iran: progress from embryonic oceanic lithosphere into magmatic arc constrained by new isotopic and geochemical data. Lithos 210, 224–241.

Moghadam, H.S., Griffin, W.L., Li, X.H., Santos, J.F., Karsli, O., Stern, R.J., Ghorbani, G., Gain, S., Murphy, R., O'Reilly, S.Y., 2017b. Crustal evolution of NW Iran: Cadomian arcs, Archean fragments and the Cenozoic magmatic flare-up. J. Petrol. 58, 2143–2190.

Moghadam, H.S., Khademi, M., Hu, Z.C., Stern, R.J., Santos, J.F., Wu, Y.B., 2015. Cadomian (Ediacaran-Cambrian) arc magmatism in the ChahJam-Biarjmand metamorphic complex (Iran): magmatism along the northern active margin of Gondwana. Gondwana Res. 27, 439–452.

Moghadam, H.S., Li, X.-H., Griffin, W.L., Stern, R.J., Thomsen, T.B., Meinhold, G., Aharipour, R., O'Reilly, S.Y., 2017c. Early Paleozoic tectonic reconstruction of Iran: tales from detrital zircon geochronology. Lithos 268, 87–101.

Moghadam, H.S., Li, X.-H., Santos, J.F., Stern, R.J., Griffin, W.L., Ghorbani, G., Sarebani, N., 2017d. Neoproterozoic magmatic flare-up along the N. margin of Gondwana: the Taknar complex, NE Iran. Earth Planet. Sci. Lett. 474, 83–96.

Muntener, O., Kelemen, P.B., Grove, T.L., 2001. The role of H2O during crystallization of primitive arc magmas under uppermost mantle conditions and genesis of igneous pyroxenites: an experimental study. Contrib. Mineral. Petrol. 141, 643–658.

Otamendi, J.E., Pinotti, L.P., Basei, M.A.S., Tibaldi, A.M., 2010. Evaluation of petrogenetic models for intermediate and silicic plutonic rocks from the Sierra de Valle Fertil-La Huerta, Argentina: petrologic constraints on the origin of igneous rocks in the Ordovician Famatinian-Puna paleoarc. J. South Am. Earth Sci. 30, 29–45.

Paterson, S.R., Ducea, M.N., 2015. Arc magmatic tempos: gathering the evidence. Elements 11, 91–97.

Pereira, M.F., Sola, A.R., Chichorro, M., Lopes, L., Gerdes, A., Silva, J.B., 2012. North-Gondwana assembly, break-up and paleogeography: U-Pb isotope evidence from detrital and igneous zircons of Ediacaran and Cambrian rocks of SW Iberia. Gondwana Res. 22, 866–881.

Plank, T., Langmuir, C.H., 1998. The chemical composition of subducting sediment and its consequences for the crust and mantle. Chem. Geol. 145, 325–394.

Puelles, P., Ibarguchi, J.G., Beranoaguirre, A., Ábalos, B., 2012. Mantle wedge deformation recorded by high-temperature peridotite fabric superposition and hydrous retrogression (Limo massif, Cabo Ortegal, NW Spain). Int. J. Earth Sci. 101, 1835–1853.

Rahmati-Ilkhchi, M., Jerabek, P., Faryad, S.W., Koyi, H.A., 2010. Mid-Cimmerian, Early Alpine and Late Cenozoic orogenic events in the Shotur Kuh metamorphic complex, Great Kavir block, NE Iran. Tectonophysics 494, 101–117.

Rudnick, R., Gao, S., 2003. The composition of the continental crust. In: Treatise on Geochemistry, vol. 3, p. 659.

Schmidt, M.W., 1992. Amphibole composition in tonalite as a function of pressure: an experimental calibration of the Al-in-hornblende barometer. Contrib. Mineral. Petrol. 110, 304–310.

Stern, R.J., Ali, K.A., Ren, M., Jarrar, G.H., Romer, R.L., Leybourne, M.I., Whitehouse, M.J., Ibrahim, K.M., 2016. Cadomian (∼560 Ma) crust buried beneath the northern Arabian Peninsula: mineral, chemical, geochronological, and isotopic constraints from NE Jordan xenoliths. Earth Planet. Sci. Lett. 436, 31–42.

Stern, R.J., Tamura, Y., Ishizuka, O., Shukano, H., Bloomer, S.H., Embley, R.W., Leybourne, M., Kawabata, H., Nunokawa, A., Nichols, A.R., 2014. Volcanoes of the Diamante cross-chain: evidence for a mid-crustal felsic magma body beneath the Southern Izu–Bonin–Mariana arc. Geol. Soc. (Lond.) Spec. Publ. 385, 235–255.

Stern, R.J., Tamura, Y., Shukuno, H., Miyazaki, T., 2019. The Zealandia Volcanic complex: further evidence of a lower crustal “hot zone” beneath the Mariana Intraoceanic Arc, Western Pacific. Isl. Arc. 28 (5), e12308.

Stuart, C., Daczko, N., Piazolo, S., 2016. Local partial melting of the lower crust triggered by hydration through melt–rock interaction: an example from Fiordland, New Zealand. J. Metamorph. Geol.

Tilhac, R., Ceuleneer, G., Griffin, W.L., O'Reilly, S.Y., Pearson, N.J., Benoit, M., Henry, H., Girardeau, J., Grégoire, M., 2016. Primitive arc magmatism and delamination: petrology and geochemistry of pyroxenites from the Cabo Ortegal complex, Spain. J. Petrol. 57, 1921–1954.

Ustaomer, P.A., Ustaomer, T., Gerdes, A., Robertson, A.H.F., Collins, A.S., 2012. Evidence of Precambrian sedimentation/magmatism and Cambrian metamorphism in the Bitlis Massif, SE Turkey utilising whole-rock geochemistry and U-Pb LA-ICP-MS zircon dating. Gondwana Res. 21, 1001–1018.

Verdel, C., Wernicke, B.P., Ramezani, J., Hassanzadeh, J., Renne, P.R., Spell, T.L., 2007. Geology and thermochronology of Tertiary Cordilleran-style metamorphic core complexes in the Saghand region of central Iran. Geol. Soc. Am. Bull. 119, 961–977.

Walker, B.A., Bergantz, G.W., Otamendi, J.E., Ducea, M.N., Cristofolini, E.A., 2015. A MASH zone revealed: the Mafic Complex of the Sierra Valle Fertil. J. Petrol. 56, 1863–1896.

Watson, E.B., Wark, D.A., Thomas, J.B., 2006. Crystallization thermometers for zircon and rutile. Contrib. Mineral. Petrol. 151, 413–433.